AD_____

Award Number: DAMD17-01-1-0331

TITLE: Prediction of Chemotherapy Response by Magnetic Resonance Spectroscopy

PRINCIPAL INVESTIGATOR: Michael Garwood, Ph.D.

CONTRACTING ORGANIZATION: University of Minnesota
Minneapolis, Minnesota 55455-2070

REPORT DATE: October 2003

TYPE OF REPORT: Annual

PREPARED FOR: U.S. Army Medical Research and Materiel Command
Fort Detrick, Maryland 21702-5012

DISTRIBUTION STATEMENT: Approved for Public Release;
Distribution Unlimited

The views, opinions and/or findings contained in this report are those of the author(s) and should not be construed as an official Department of the Army position, policy or decision unless so designated by other documentation.

REPORT DOCUMENTATION PAGE

Form Approved
OMB No. 074-0188

1. AGENCY USE ONLY (Leave blank)	2. REPORT DATE	3. REPORT TYPE AND DATES COVERED
	October 2003	Annual (17 Sep 2002 - 16 Sep 2003)

4. TITLE AND SUBTITLE
Prediction of Chemotherapy Response by Magnetic Resonance Spectroscopy

5. FUNDING NUMBERS
DAMD17-01-1-0331

6. AUTHOR(S)
Michael Garwood, Ph.D.

7. PERFORMING ORGANIZATION NAME(S) AND ADDRESS(ES)
University of Minnesota
Minneapolis, Minnesota 55455-2070

E-Mail: gar@cmrr.umn.edu

8. PERFORMING ORGANIZATION REPORT NUMBER

9. SPONSORING / MONITORING AGENCY NAME(S) AND ADDRESS(ES)
U.S. Army Medical Research and Materiel Command
Fort Detrick, Maryland 21702-5012

10. SPONSORING / MONITORING AGENCY REPORT NUMBER

11. SUPPLEMENTARY NOTES

12a. DISTRIBUTION / AVAILABILITY STATEMENT
Approved for Public Release; Distribution Unlimited

12b. DISTRIBUTION CODE

13. ABSTRACT (Maximum 200 Words)

This research seeks to validate the use of a non-invasive tool, in vivo magnetic resonance spectroscopy (MRS), to assess therapeutic response in patients with locally-advanced breast cancer who receive primary systemic therapy (PST), also know as neoadjuvant chemotherapy. Contrast-enhanced MRI was used to measure tumor size and MRS was used to monitor tumor concentrations of choline-containing compounds [tCho] known to be elevated in cancers and in cell proliferation. To date, 13 women have been followed with MRS and MRI through the complete course of PST (ACx4). Clinical response assessment by MRI was based on the response evaluation criteria in solid tumors (RECIST). Changes in [tCho] between the baseline scan (<1 wk before starting AC) and 24 hours after the 1st cycle of AC showed a significant positive correlation with change in tumor size measured after 4 cycles of AC ($R=0.89$, $p<0.0001$). Opposite trends in [tCho] between objective responders and nonresponders ($p=0.0101$) were observed already at 24 hours after starting PST. These results show that MRS can distinguish responders versus nonresponders early in the course of PST. These findings provide evidence that MRS can be used clinically to individualize treatments for maximizing benefit and to rapidly assess efficacy of new drugs.

14. SUBJECT TERMS
Magnetic resonance spectroscopy, metabolic imaging, chemotherapy

15. NUMBER OF PAGES
73

16. PRICE CODE

17. SECURITY CLASSIFICATION OF REPORT	18. SECURITY CLASSIFICATION OF THIS PAGE	19. SECURITY CLASSIFICATION OF ABSTRACT	20. LIMITATION OF ABSTRACT
Unclassified	Unclassified	Unclassified	Unlimited

Table of Contents

INTRODUCTION

Adjuvant chemotherapy reduces the risk of breast cancer death for essentially all stages of the disease, although the absolute benefits of chemotherapy are small. The development of many new effective agents may provide several improved options for many women. A major challenge in breast cancer treatment is to determine which chemotherapeutic agent will provide the most benefit for an **individual** patient. Effective chemotherapy inhibits cell proliferation and induces apoptosis. Previous research has shown that elevated levels of choline-containing compounds (tCho) in cancer cells are linked to high proliferation. In vivo tumor concentrations of tCho, [tCho], can be measured non-invasively using in vivo magnetic resonance spectroscopy (MRS). The objective of this research is to determine whether in vivo MRS measurements of [tCho] can identify chemotherapy-induced growth arrest, and possibly apoptosis, in patients with locally-advanced breast cancer (LABC) who receive primary systemic therapy (PST), also known as neoadjuvant chemotherapy. The goal is to determine whether changes in [tCho] can identify responders and non-responders very early in the course of treatment (within 24 hr – 3 wks). The study employs a MR scanner having a high magnetic field (4 Tesla) which improves the sensitivity for [tCho] measurement. To measure tumor size changes and to locate the tumors for [tCho] measurements, the protocol also includes contrast-enhanced MRI scanning. MRS measurements of [tCho] are compared with clinical response based on tumor size changes by MRI and by pathological evaluation of the surgically-resected tissue after PST . This research is expected to show that MRS can be used to individualize and optimize adjuvant chemotherapy regimens for the treatment of breast cancer.

BODY

Our major efforts continue to be engaged in Task 1: Monitoring changes in [tCho] by MRS and tumor size by MRI in response to PST. In the period of time since gaining approval by the HSRRB to use human subjects (January 2002), we have enrolled 22 patients in the study.

We are also engaged in Task 2: Analyzing data collect under Task 1 to determining how changes in MRS correlate with tumor response detected by MRI and with pathology findings. The MRS and MRI data from 13 patients that were followed through a complete course of PST have been analyzed. The results are extremely exciting, since the MRS measured changes in [tCho] appear to predict clinical response consistently very early in the course of treatment. Changes in [tCho] between the baseline scan (acquired within 1 wk before starting PST) and 24 hours after the first cycle of PST showed a significant positive correlation with change in tumor size (longest dimension, LD) after 4 cycles of doxorubicin-based PST ($R=0.89$, $p<0.0001$). Opposite trends in [tCho] changes between objective responders and nonresponders ($p=0.0101$) were observed already by 24 hours after starting PST. The details of these findings are described in a manuscript entitled "Predicting Response to Neoadjuvant Chemotherapy of Locally Advanced Breast Cancer with In Vivo 1H MRS: A Pilot Study at 4 Tesla", which is included in the Appendix. In this manuscript, the plots in figures 1, 3, and 5 show the most relevant data. This manuscript has been submitted to a peer-reviewed journal, *Radiology*, and is currently under review. In addition, we recently submitted an abstract

describing these early results for presentation at the annual meeting of the Radiological Society of North America (RSNA), to be presented by our senior Research Associate working on the project, Sina Meisamy, M.D. We have received notice that the abstract has been accepted for presentation on December 2, and based on this work, Dr. Meisamy will be awarded the RSNA Resident Research Trainee Prize, to be honored at the time of presentation.

MRS methodology able to quantify tCho in breast lesions is crucial to this project. Although the development of this methodology was not one of the specific Tasks in this project, the data generated as part of Task 1 could be used to help validate our tCho quantification procedure. A manuscript describing our quantitative MRS methodology entitled "In Vivo Quantification of Choline Compounds in the Breast with 1H MR Spectroscopy" was submitted to the peer-reviewed journal, *Magnetic Resonance in Medicine*. We recently learned that the manuscript was favorably reviewed (in fact, both referees gave it outstanding ratings) and is expected to appear in an early 2004 issue of the journal. A preprint is included in the Appendix.

KEY RESEARCH ACCOMPLISHMENTS

- We have shown that the concentration change of choline-containing compounds in the tumors (baseline versus 24 hours after the 1st cycle of chemotherapy) predicts clinical response (as determined by the change in tumor size measured by MRI; baseline versus 4 cycles of chemotherapy).
- These results suggest that MRS can be used clinically to distinguish responders versus nonresponders early in the course of neoadjuvant chemotherapy..

REPORTABLE OUTCOMES

Manuscripts:

S. Meisamy, P.J. Bolan, E.H. Baker, E. Gulbahce, L.I. Everson, M.T. Nelson, T. Emory, T. Tuttle, D. Yee, and M. Garwood, "Predicting Response to Neoadjuvant Chemotherapy of the Locally Advanced Breast Cancer with In Vivo 1H MRS: A Pilot Study at 4 Tesla", submitted to *Radiology*

P.J. Bolan, S. Meisamy, E.H. Baker, J. Lin, T. Emory, M. Nelson, L.I. Everson, D. Yee, and M. Garwood, "In Vivo Quantification of Choline Compounds in the Breast with 1H MR Spectroscopy", accepted for publication in *Magn. Reson. Med.*

Abstract:

S. Meisamy, P.J. Bolan, J.C. Lin, L.I. Everson, M.T. Nelson, T. Emory, D. Yee, and M. Garwood, "The Value of Adding MRS to MRI for Predicting Response to Neoadjuvant Chemotherapy of Locally Advanced Breast Cancer: A Pilot Study at High Field", to be presented at the Annual Meeting of the RSNA, December 2003.

CONCLUSIONS

Clinical response can be predicted as early as 24 hours after the 1st cycle of doxorubicin-based chemotherapy using in vivo MRS measurement of choline-containing compounds in the tumor. These findings are highly significant because they show that MRS can distinguish responders versus nonresponders early in the course of treatment and suggest the use of MRS clinically to individualize treatments for maximizing benefit and to rapidly assess efficacy of new drugs.

REFERENCES

None

APPENDICES

Attached

PREDICTING RESPONSE TO NEOADJUVANT CHEMOTHERAPY OF LOCALLY ADVANCED BREAST CANCER WITH *IN VIVO* ^{1}H MRS: A PILOT STUDY AT 4 TESLA

Sina Meisamy, M.D.[1,2], Patrick J Bolan, B.S. [1,2], Eva H. Baker, M.D., Ph.D. [1,2], Evin Gulbahce, M.D.[3], Lenore I Everson, M.D.[2], Michael T. Nelson, M.D. [2], Tim Emory, M.D. [2], Todd Tuttle, M.D. [4], Douglas Yee, M.D. [5,6], Michael Garwood, Ph.D. [1,2,5,*]

[1]The Center for Magnetic Resonance Research, [2]Department of Radiology, [3]Department of Pathology/Laboratory Medicine, [4]Department of Surgery, [5]Cancer Center, [6]Department of Medicine, University of Minnesota School of Medicine, Minneapolis, Minnesota, USA

*Send Correspondence to:

Michael Garwood, Ph.D.
Center for Magnetic Resonance Research
2021 Sixth Street SE
Minneapolis, MN 55455
Email: gar@cmrr.umn.edu
Phone: 612-626-2001
Fax: 612-626-2004

Please note that this work has been originated from the same address as the address of the corresponding author.

**This original research is scheduled to be presented at the 2003 RSNA meeting December 2nd, 2003 at 3:20 PM. The abstract ID is 101628 and paper number is 750.

** This original research won the research trainee prize at the 2003 RSNA

Grants:

- DOD Breast Cancer Research Program DAMD 17-01-1-0331
- NIH grants RR08079, CA92004, RR00400
- Tickle Family Land Grant Endowment in Breast Cancer Research
- PHS Cancer Center Support Grant P30 CA77398

Abstract

Purpose: The purpose of this study was to determine whether changes in total choline concentration ([tCho]) before and within 24 hours after primary (neoadjuvant) systemic therapy (PST) predicted clinical response in patients with locally advanced breast cancer (LABC).

Materials and Methods: Sixteen women with biopsy-confirmed LABC scheduled for doxorubicin-based PST were recruited. Using a 4T MR scanner, subjects were scanned prior to treatment and within 24 hours after the first cycle of PST. Lesions were visualized with fat-suppressed 3D FLASH and assessed by time-course of Gd -DTPA uptake with fat-suppressed 2D multislice FLASH. Levels of choline-containing metabolites (tCho) were quantified using ^{1}H MR spectroscopy. Each scan was evaluated for lesion size and [tCho].

Results: Fourteen of 16 patients completed the protocol. [tCho] was not obtained in one patient because irregular lesion morphology prevented suitable tCho measurements. Of the remaining thirteen patients, 10 had invasive ductal carcinoma (IDC), 2 had invasive lobular carcinoma (ILC), and 1 had mixed IDC/ILC. Based on RECIST criteria, 8/13 patients had an objective response and 5/13 were nonresponders. Changes in [tCho] between the baseline scan and 24 hours after the first cycle of PST showed a significant positive correlation with changes in tumor size ($R = 0.89$, $p < 0.0001$) and was significantly different between objective responders and nonresponders ($p = 0.0101$).

Conclusion: These results suggest that changes in [tCho], between the baseline scan and within 24 hours after the first cycle of PST, can serve as an important indicator for predicting clinical response in LABC.

Introduction

Primary systemic therapy (PST), also known as neoadjuvant chemotherapy, given prior to breast cancer surgery offers several advantages over standard post-operative chemotherapy. Although PST does not offer any survival benefits over post-operative chemotherapy (1, 2), patients who receive PST are more likely to receive breast conserving surgery. Moreover, the use of PST permits *in vivo* monitoring of tumor response. One study demonstrated that complete disappearance of tumor at surgical resection (pathologic complete response) was associated with the best overall survival (2). This observation has been confirmed by other PST studies suggesting that pre-operative chemotherapy has distinct benefits (3, 4). Furthermore, since there are many active agents in breast cancer, it is important to know early in the course of treatment whether the drug chosen will be effective for that patient.

Currently there are no standardized criteria that can individually predict response to PST. Conventional modalities such as physical examination, ultrasonography, and mammography vary in reliability for measuring tumor response (5-8). One study revealed that patients' response after a complete course of PST correlated with physical examination, ultrasonography, and conventional mammography in 47%, 66%, and 49% of the cases, respectively (8). MRI has become increasingly used in patients with locally advanced breast cancer (LABC). With respect to treatment monitoring, studies have shown correlation between specific MRI findings and clinical response. Researchers have shown that changes in tumor size, tumor phenotype, dynamic contrast enhancement,

and extraction flow product all correlate with clinical response (9-15). However, changes seen in both tumor size and dynamic contrast enhancement measured by MRI are not detected until at least 6 weeks following PST (13). The ability to immediately detect response to a specific chemotherapeutic regimen would be ideal, since it would allow for optimal individualization of chemotherapeutic regimens for patients with the goal of obtaining a pathologic complete response.

Recently there has been an interest in investigating the use of magnetic resonance spectroscopy (MRS) for detecting and monitoring patients with cancer. Using MRS, it has been shown that breast tissue containing neoplastic cells have elevated choline-containing metabolites (tCho), which yield a signal at 3.2 ppm in the proton (^{1}H) spectrum (16-19). Other groups have shown how a decrease or disappearance of the tCho signal after administration of PST may potentially be used to predict response in LABC (20). Another group showed a correlation between the change in tCho signal and clinical response in patients with extracranial lymphomas and germ cell tumors (21).

MRS of the breast is technically challenging because sensitivity can be limiting and spectral artifact can occur. Due to the heterogeneous distribution of fat and glandular tissue in the breast, ^{1}H spectra of breast often contain large lipid signals that give rise to contaminant peaks around 3.2 ppm. Fortunately, these artifact peaks, otherwise known as sidebands, can be suppressed by using a recently developed technique called echo-time (TE) averaging (22). Additionally, treatment monitoring requires implementation of a spectral quantification method. Previous studies at lower magnetic field strength (1.5 T)

assumed that tCho is detectable only in malignant breast tissue. Here, a quantitative technique is used to determine tCho concentration ([tCho]) in breast tumors *in vivo* (23).

In this study, it was hypothesized that an early decrease in [tCho] could identify early response to PST. The purpose of this study was to evaluate whether the change in the [tCho], as quantified by single voxel ^{1}H MRS, before treatment and within 24 hours after the first cycle of PST, predicted clinical response in patients with LABC.

Materials and Methods:

Patients

Patients between the ages of 18 - 80 years old with biopsy-confirmed LABC who were scheduled to receive doxorubicin-based PST were eligible to enroll in our prospective study. The study was approved by the Institutional Review Board at the University of _ _____, School of Medicine. Informed written consent was obtained prior to all studies. Patients were referred by medical oncologists working at the University of_____ or in private practice. Treatment consisted of standard adriamycin and cyclophosphamide (AC) regimen (doxorubicin – 60 mg/m^2, cyclophosphamide 600 mg/m^2) given on day 1. Patients were scanned prior to treatment and within 24 hours of the first cycle of AC. Patients had the option of returning for additional scans after each cycle of treatment. Patients received a final scan after the last cycle of AC. Patients received their first cycle of AC at a median of 2 days (range 1-5 days) after their baseline scan.

MRI and MRS techniques

All measurements were performed with a hybrid 4T system, consisting of a 90cm bore magnet (model 4T - 900, Oxford Magnet Technology, Oxford shire, UK) with a clinical gradient system (model 'Sonata', Siemens, Erlangen, Germany) interfaced with an imaging spectrometer (model 'Unity Inova', Varian, Palo Alto, CA). The gradient system was capable of 40mT/m with a 400μs rise time. Several different single-breast quadrature transmit/receive RF surface coils of similar design were used to accommodate different breast sizes. The coils were mounted onto a custom-built patient table designed for unilateral, prone breast studies. Patients were positioned prone with their breast centered horizontally in the magnet. After acquiring scout images to verify position, the coil was manually tuned and matched. A high-resolution 3D FLASH image (fat-suppressed, matrix = 256 x 256 x 64, field of view = 14-18 cm, TE/TR = 4.1/13.5 ms, flip angle = 30°) and a fast 2D multislice image (fat-suppressed, matrix = 256 x 128, 30 slices, slice thickness = 2.5 mm, field of view = 14-18 cm, TE/TR = 5.1/390 ms, flip angle = 90°) were acquired prior to injection of Gd- DTPA (0.1 mmol/kg body weight). Five sets of 2D images were acquired immediately after injection, followed by a second 3D image acquisition. Both image sets were analyzed using our own image processing software (developed with Matlab; The Mathworks, Natick, MA) to select voxels for MRS with the subject still in the magnet.

Criteria for voxel selection included lesion architecture, dynamic contrast uptake, and prior clinical knowledge from mammographic or ultrasound images. Voxels were planned to maximize coverage of the lesion while minimizing inclusion of adipose tissue.

Voxels which were planned in studies following PST were placed in the same area as those in the baseline scan. If the lesion changed in size in the scans following PST, the voxel would be planned to maximize coverage of the new lesion size. Single-voxel spectroscopy was performed with the LASER technique (24) using 4096 complex points and 6 kHz spectral width. Each voxel measurement began with a calibration of the localized B_1 field strength, followed by 30-60 s of manual adjustment of the linear shims. A fully relaxed, single-shot, unsuppressed spectrum was acquired to measure the water and lipid peaks. The power required to suppress the water signal using VAPOR (25) suppression was then manually adjusted. The metabolite spectrum was acquired using TE averaging with TE = 45-196 ms in 64 or 128 increments with TR=3 s (22). Each free induction decay signal was individually saved – no averaging was performed until processing. Levels of [tCho] were quantified by fitting the data to a Voigt lineshape model and using unsuppressed water as an internal reference (23). All [tCho] measurements were recorded in units of mmol/kg water.

Data and Statistical Analysis

Tumor sizes measured by MRI were based on longest diameter (LD). Tumor size was measured at baseline (LD_0) and after the last cycle of AC (LD_f). The percent LD_f relative to baseline level ($\%LD_f$) was calculated according to:

$$\%LD_f = 100\left(\frac{LD_f}{LD_0}\right) \quad [1]$$

The percent change in tumor size ($\%\Delta LD$), between LD_0 and LD_f, was calculated by using the equation:

$$\%\Delta LD = 100\left(\frac{(LD_f - LD_0)}{LD_0}\right) \quad [2]$$

Levels of [tCho] were measured at baseline ($[tCho]_0$) and within 24 hours of the first cycle of AC ($[tCho]_{24}$). The percent $[tCho]_{24}$ relative to the baseline level ($\%[tCho]_{24}$) was calculated according to:

$$\%[tCho]_{24} = 100\left(\frac{[tCho]_{24}}{[tCho]_0}\right) \quad [3]$$

The percent change in [tCho] ($\%\Delta[tCho]$), between $[tCho]_0$ and $[tCho]_{24}$, was calculated using the equation:

$$\%\Delta[tCho] = 100\left(\frac{[tCho]_{24} - [tCho]_0}{[tCho]_0}\right) \quad [4]$$

Using the classification system of the Response Evaluation Criteria in Solid Tumors (RECIST) (26), patients were categorized into two groups: objective responders and nonresponders. Objective responders were patients who had greater than a 30% decrease in LD. Nonresponders were patients who had less than 30% decrease, no change, or increase in LD after the final dose of AC. The association between the $\%\Delta[tCho]$ and the $\%\Delta LD$ was calculated by using Pearson's correlation coefficient (27). The association between $\%\Delta[tCho]$ and patient response was calculated by using the Wilcoxon rank-sum test (28).

Results:

Patient and Tumor Characteristics

A total of 16 patients were recruited, of which 14 completed the protocol. Two patients did not complete the study because one opted to have surgery prior to completing all four cycles of PST and the second patient decided not receive PST and instead chose an alternative method of treatment. Among the 14 patients who completed the study, 1 patient was not included in the data analysis because of inadequate MRS measurements.

A summary of the patients' tumor characteristics, [tCho], and clinical response are shown in Table 1. The median age of the patient group was 46 years old (range 31-70 years). Eight of 13 patients were premenopausal of which 5 had a prior history of taking oral contraceptives. Five of 13 patients were postmenopausal of which 2 were on hormone replacement therapy. Histologic diagnosis was obtained by ultrasound guided needle core biopsy in 11/13 patients and by mammographic stereotactic guided biopsy in 2/13 patients.

The median LD_0 was 4.4 cm (range 2.1-9.5 cm). The median LD_f for objective responders and nonresponders was 1.9 cm (range 0-4.2 cm) and 5.0 cm (range 2.7-9.5 cm), respectively. The median $[tCho]_0$ was 3.0 mmol/kg (range 1.0-8.5 mmol/kg). The median $[tCho]_{24}$ for objective responders and nonresponders was 2.6 mmol/kg (range 0-6.1 mmol/kg) and 1.9 mmol/kg (range 1.1-3.4 mmol/kg), respectively.

Objective Response

Eight of 13 patients experienced an objective response with diminished tumor size. LD decreased by a median of 61% (range 35-100%) after 4 cycles of AC, whereas [tCho]

decreased by a median of 40% (range 20-100%) within 24 hours of receiving the first cycle of AC. All 8 patients who were objective responders had a $[tCho]_{24}$ which was less than $[tCho]_0$, (Table 1). Figure 1 shows $[tCho]_{24}$ and LD_f as a percent of the baseline for the objective responders. For each patient, $\%LD_f$ and $\%[tCho]_{24}$ were calculated as a percent of the baseline by using equations 1 and 3, respectively.

Figure 2 shows MR data from an objective responder. The patient was a 43 year old African American female who was diagnosed with invasive ductal carcinoma (IDC) with positive lymph nodes. The patient was initially treated with four cycles of AC. At baseline, $[tCho]_0$ was 4.6 mmol/kg and LD_0 was 4.0 cm. Twenty-four hours after the first cycle of AC, $[tCho]_{24}$ dropped to 3.7 mmol/kg while LD remained at 4.0 cm. At that point, $\%\Delta[tCho]$ was -20% and it was predicted that the patient would have an objective response. Twelve weeks later, after the fourth cycle of AC, [tCho] decreased to 0.9 mmol/kg and LD_f was 1.7 cm. Based on $\%\Delta LD$, which was -58%, the patient was classified as an objective responder. This patient had palpable lymphadenopathy . Since treatment with paclitaxel is regarded as standard therapy for node-positive patients (29), it was elected that this patient continue on systemic therapy prior to surgery. Interestingly, twenty-four hours after the second cycle of paclitaxel, [tCho] increased to 4.1 mmol/kg and LD remained at 1.7 cm.

No Response

Five of 13 patients were nonresponders. After 4 cycles of AC, LD decreased in 3/5 patients by a median of 10% (range 7-13%), increased in 1/5 patients by 6% and did not

change in 1/5 patients. Within 24 hours after the first cycle of AC, [tCho] increased in 4/5 patients by a median of 34% (range 10-50 %) and did not change in 1/5 patients. All 5 patients who were nonresponders had a $[tCho]_{24}$ which was greater than or equal to the $[tCho]_0$, (Table 1). Figure 3 shows $[tCho]_{24}$ and LD_f as a percent of the baseline for the nonresponders.

Figure 4 shows MR data of a nonresponder. The patient was a 42 year old white female who was diagnosed with IDC. The patient was treated with four cycles of AC. At baseline, the $[tCho]_0$ was 1.4 mmol/kg and LD_0 was 2.9 cm. Twenty-four hours after the first cycle of AC, the patient's $[tCho]_{24}$ increased to 2.1 mmol/kg while LD remained at 2.9 cm. At that point, %Δ[tCho] was 50% and it was predicted that the patient would be a nonresponder. Twelve weeks later, after the fourth cycle of AC, the patient's [tCho] was 0.9 mmol/kg and LD_f was 2.7 cm. Based on %ΔLD of only -7%, this patient was classified as a nonresponder.

Correlation between %Δ[tCho] and %ΔLD

%Δ[tCho] shows a significant positive correlation with %ΔLD ($R = 0.89$, $p < 0.0001$). Figure 5 is a graph of the correlation between %Δ[tCho] and %ΔLD. The points on the graph are separated into 2 groups: objective responders and nonresponders, based on the RECIST criteria. All 5 patients who were nonresponders (black squares) had a %Δ[tCho] that was greater than or equal to zero. All 8 patients who had an objective response (white squares) had a %Δ[tCho] that was less than zero. The %Δ[tCho] was significantly

different between objective responders and nonresponders (Wilcoxon rank-sum test, $p = 0.0101$).

Discussion:

This pilot study shows that MRS predicts clinical response within 24 hours of the first cycle of PST. These results suggest that the addition of high field ^1H MRS can offer a significant advantage over using MRI alone in predicting response to PST.

All patients who were objective responders had a lower $[tCho]_{24}$ as compared to $[tCho]_0$. Perhaps, the immediate decrease in [tCho] may be caused by the acute cytotoxic effect of doxorubicin. Furthermore, all patients who were nonresponders had either no change or a higher $[tCho]_{24}$ as compared to $[tCho]_0$. This may be related to the fact that certain breast tumors exhibit *de novo* resistance to doxorubicin and as a result, PST with the AC regimen would have no effect on the proliferating tumor cells.

Within 24 hours after the first cycle of PST, [tCho] dropped in all objective responders and the smallest absolute decrease was 20%. All nonresponders except one had a measurable increase in [tCho] within 24 hours after the first cycle of PST. Obviously, the ability to measure [tCho] accurately was fundamental to the success of this project. The accuracy of [tCho] measurements depends most directly on the signal-to-noise ratio (SNR) which has been shown to increase at least linearly with magnetic field strength (30, 31). Thus, the 4T scanner used here offered a significant advantage. Further studies

are needed to determine whether 1.5T scanners can provide the SNR necessary to measure [tCho] accurately. However, newer 3T clinical scanners are expected to perform similar to the 4T scanner used here.

The ability of MRS to predict clinical response might be of limited value when attempting measurements on small or irregularly shaped tumors. The accuracy of the [tCho] measurement is limited primarily by SNR, especially in voxels less than 1 cm^3. Fortunately, the minimum voxel size used for monitoring response to PST will typically be significantly greater than 1 cm^3, since tumors must be at least 2 cm in LD (Stage II or higher) to be eligible for PST. Another source of error in [tCho] measurements arises when intense lipid signals are present in the voxel (22). Breast tumors with thin or linear morphology can pose significant problems for the spectroscopist planning the voxel. For example, in this study data from one patient was excluded from the analysis due to an inability to plan a suitable voxel for [tCho] measurements at baseline and following PST. The patient was a 49 year old white female who was diagnosed with inflammatory breast cancer. At baseline, the MRI revealed a 6 cm tumor which was diffuse and linear in shape. Even though the tumor was 6 cm in LD, its linear portion was at maximum 0.3 cm thick. Due to its thin morphology, it was not possible to plan a rectangular voxel containing less than 30% fat by volume, as required by the quantification method (23). This unusual tumor, characterized by diffuse enhancement and linear shape, was the only one of its type encountered in the study so far.

It is expected that quantitative ^{1}H MRS will not only improve the accuracy of MRI in detecting breast cancer, but as shown here it can be used with MRI to assess PST response early in the course of treatment. Quantification of the tCho peak is also expected to aid health care professionals who lack the experience in reading and interpreting MR spectra.

$[tCho]_0$ and $[tCho]_{24}$ independently showed no correlation with LD_0 or LD_f. $[tCho]_0$ showed no significant correlation with tumor histology or MRI morphology. However, our data are in agreement with a previous report describing the association between breast tumor phenotype on MRI and response (9). In this study, 4/8 patients with an objective response had well circumscribed focal masses while 4/5 patients who were nonresponders had nodular, patchy, and diffuse enhancement characteristics on MRI. $[tCho]_0$ independently showed no significance in predicting clinical response. Furthermore, there was no significant difference in $[tCho]_{24}$ between objective responders and nonresponders.

The precise mechanism as to why neoplastic tissues exhibit elevated tCho levels still remains unanswered. It has been proposed that the increase pools of tCho in neoplastic tissue is not only due to the high cell membrane synthesis, which is associated with accelerated tumor cell replication, but it may also be from the interaction between biosynthetic and catabolic events of tumor cells by which tCho acts as both precursors and catabolites (32). Others have observed that the that the predominant intracellular mechanism responsible for the augmented levels of phosphocholine, the primary

metabolite responsible for the (tCho) peak in neoplastic tissue, is due to up-regulation of the enzyme - choline kinase (33).

Although no other PST regimen, other than AC, was considered in this study, it is interesting to note the pattern of change in [tCho] for the patient in figure 2. Despite the fact that this individual was an objective responder to AC, it appears that the patient was not responding to paclitaxel. Between the last cycle of AC (figure 2-c) and the second cycle of paclitaxel (figure 2-d), the patient's [tCho] increased by 455%, from 0.9 to 4.1 mmol/kg, whereas the tumor size did not change. Although not shown in the figure, the patient's tumor size, even after the fourth cycle of paclitaxel, remained at 1.7 cm. This shows that early changes seen in ^{1}H MRS may even be used in predicting clinical response between different regimens.

The observation of consistent trends in the %Δ[tCho] between objective responders and nonresponders suggest that *in vivo* ^{1}H MRS, with MRI, may be a highly sensitive indicator in predicting clinical response as early as 24 hours after the first cycle of PST. Monitoring patients on PST with MRS appears to offer a means to detect the presence of viable and/or proliferating neoplastic tumor cells. With the possibility of early prediction comes the benefit of immediate assessment in tailoring an effective regimen for a specific individual. Perhaps early changes seen in ^{1}H MRS of breast cancer patients who undergo PST may even serve as an indicator of risk for recurrent or metastatic breast cancer. Furthermore, the opportunity for such early prediction will be highly advantageous for

researchers seeking to evaluate new PST drugs and may help to elucidate the mechanisms of multi drug resistance in breast cancer.

These promising findings were obtained from a small group of patients and thus a study of a larger prospective patient series is needed. A larger study may also provide information about the possibility of using MRS to predict when a patient is destined to have a pathologic complete response. To the best of our knowledge, this is the first report in which quantitative tCho measurements were made with *in vivo* ^{1}H MRS for the purpose of predicting clinical response in breast cancer patients who undergo PST.

References

1. Fisher B, Brown A, Mamounas E, et al. Effect of preoperative chemotherapy on local-regional disease in women with operable breast cancer: Findings from national surgical adjuvant breast and bowel project B-18. J Clin Oncol 1997; 15:2483-2493.
2. Fisher B, Bryant J, Wolmark N, et al. Effect of preoperative chemotherapy on outcome of women with operable breast cancer. J Clin Oncol 1998; 16:2672-2685.
3. Smith IC, Heys SD, Hutcheon AW, et al. Neoadjuvant chemotherapy in breast cancer: significantly enhanced response with docetaxel. J Clin Oncol 2002; 20:1456-1466.
4. Kaufmann M, Von Minckwitz G, Smith R, et al. International expert panel on the use of primary (preoperative) systemic treatment of operable breast cancer: review and recommendations. J Clin Oncol 2003; 21:2600-2608.
5. Junkerman H, Founier D. Imaging procedures for assessment of the response of mammary carcinoma to preoperative chemotherapy. Radiologe 1997; 37:726-732.
6. Segel MC, Paulus DD, Hortobagyi GN. Advanced primary breast cancer: assessment at mammography response to induction chemotherapy. Radiology 1998; 169:49-54.
7. Vinnicombe SJ, Mac Vicar AD, Guy RL, Sloane JP, Powles TJ, Knee G, Husband JE. Primary breast cancer: mammographic changes after neoadjuvant chemotherapy, with pathologic correlation. Radiology 1996; 198:333-340.

8. Herrada J, Iyer RB, Atkinson EN, Sneige N, Buzdar AU, Hortobabyi GN. Relative value of physical examination, mammography, and breast sonography in evaluating the size of the primary tumor and regional lymph node metastases in women receiving neo-adjuvant chemotherapy for locally advanced breast carcinoma. Clin Cancer Res 1997; 3:1565-1569.
9. Esserman L, Kaplan E, Partridge S, et al. MRI phenotype is associated with response to doxorubicin and cyclophosphamide neoadjuvant chemotherapy in stage III breast cancer. Ann Surg Oncol 2001; 8:549-559.
10. Gilles R, Guinebretiere JM, Toussaint C, et al. Locally advanced breast cancer: contrast-enhanced subtraction MR imaging of response to preoperative neoadjuvant chemotherapy. Radiology 1994; 191:633-638.
11. Abraham DC, Jones RC, Jones SE, et al. Evaluation of neoadjuvant chemotherapeutic response of locally advanced breast cancer by magnetic resonance imaging. Cancer 1996; 78:91-100.
12. Balu-Maestro C, Chape llier C, Bluese A, Chanalet I, Chauvel C, Largillier R. Imaging in evaluation of response to neoadjuvant breast cancer treatment benefits of MRI. Breast Cancer Res Treat 2002; 72:145-152.
13. Rieber A, Brambs HJ, Gabelmann A, Heilmann V, Kreienberg R, Kühn T. Breast MRI for monitoring response of primary breast cancer to neo-adjuvant chemotherapy. Eur Radiol 2002; 12:1711-1719.
14. Choyke PL, Dwyer AJ, Knopp MV. Functional tumor imaging with dynamic contrast-enhanced magnetic resonance imaging. J Magn Reson Imaging 2003; 17:509-520.

15. Delille J, Slanetz PJ, Yeh ED, Halpern EF, Kopans DB, Garrido L. Invasive ductal breast carcinoma response to neoadjuvant chemotherapy: Noninvasive monitoring with functional MR imaging-pilot study. Radiology 2003; 228:63-69.

16. Mackinnon WB, Barry PA, Malycha PL, et al. Fine-needle biopsy specimens of benign breast lesions distinguished from invasive cancer ex vivo with proton MR spectroscopy. Radiology 1997; 204:661-666.

17. Roebuck JR, Cecil KM, Schnall MD, Lekinski RE. Human breast lesions: Characterization with proton MR spectroscopy. Radiology 1998; 209: 269-275.

18. Gribbestad IS, Sitter B, Lundgren S, Krane J, Axelson D. Metabolite composition in breast tumors examined by proton nuclear magnetic resonance spectroscopy. Anticancer Res. 1999; 19:1737-1746.

19. Kvistad KA, Bakken IJ, Gribbestad IS, et al. Characterization of neoplastic and normal human breast tissues with *in vivo* ^{1}H NMR spectra with increased magnetic field strength. J Magn Reson Imaging 1999; 10:159-164.

20. Jagannathan NR, Kumar M, Seenu V, et al. Evaluation of total choline from *in-vivo* volume localized proton MR spectroscopy and its response to neoadjuvant chemotherapy in locally advanced breast cancer. Br J Cancer 2001; 0:1-7.

21. Schwarz AJ, Maisey NR, Collins DJ, Cunningham D, Huddart R, Leach MO. Early *in vivo* detection of metabolic response: a pilot study of ^{1}H MR spectroscopy in extracranial lymphoma and germ cell tumours. Br J Radiol 2002; 75:959-966.

22. Bolan PJ, DelaBarre L, Baker EH, et al. Eliminating spurious lipid sidebands in ^{1}H MRS of breast lesions. Magn Reson Med 2002; 48:215-222.

23. Bolan PJ, Meisamy S, Baker EH, et al. *In vivo* quantification of choline compounds in the breast with ^{1}H MR Spectroscopy. Magn Reson Med – Submitted.

24. Garwood M, DelaBarre L. The return of the frequency sweep: designing adiabatic pulses for contemporary NMR. J Magn Reson Imaging 2001; 153:155-177.

25. Tkac I, Starcuk Z, Choi IY, Gruetter R. *In vivo* 1H NMR spectroscopy of rat brain at 1 msec echo time.Magn Reson Med 1999; 41:649-656.

26. Therasse P, Arbuck SG, Eisenhauer EA, et al. New guidelines to evaluate the response to treatment in solid tumors. European organization for research and treatment of cancer, National Cancer Institute of the United States, National Cancer Institute of Canada. J Natl Cancer Inst 2000; 92:205-216.

27. Le CT. Descriptive methods for continuous data. Introductory Biostatistics. Hoboken, NJ: John Wiley & Sons, Inc., 2003; 85-88.

28. Le CT. Comparison of population means. Introductory Biostatistics. Hoboken, NJ: John Wiley & Sons, Inc., 2003; 246-281.

29. Henderson IC, Berry DA, Demetri GD, et al. Improved outcomes for adding sequential paclitaxel but not from escalating doxorubicin dose in an adjuvant chemotherapy regimen for patients with node-positive primary breast cancer. J Clin Oncol 2003; 21:976-983.

30. Vaughan JT, Garwood M, Collins CM, et al. 7T vs 4T: RF power, homogeneity, and signal-to-noise comparison in head images. Magn Reson Med 2001; 46:24-30

31. Hoult DI, Richard RE. The signal-to-noise ratio of the nuclear magnetic resonance experiment. J Magn Reson Imaging 1976; 24:71-85.

32. Podo F. Tumour phospholipid metabolism. NMR Biomed 1999; 12:413-439.

33. Degani H, Rushkin E, Eliyahu G. Variations in the augmentation of phosphocholine in breast cancer; the cause and the sense (abstr). In: Proceeding of the Eleventh Meeting of the International Society for Magnetic Resonance in Medicine. Toronto, Ontario, Canada: International Society for Magnetic Resonance in Medicine, 2003; 1280.

Figure Captions

Figure 1 – Relationship between [tCho] and LD in patients with an objective response. The dashed line represents the normalized baseline value for $[tCho]_0$ and LD_0. The diamonds represent the calculated $\%[tCho]_{24}$ and the circles represent the calculated $\%LD_f$. $[tCho]_{24}$ and LD_f pairs from individual subjects are indicated by connecting lines. Notice that all the objective responders had a $[tCho]_{24}$ which was less than $[tCho]_0$.

Figure 2 – MRI and MRS of a patient with an objective response. Images are sagittal view, right breast, acquired withT1-weighed high resolution 3D FLASH using fat suppression at 7 minutes post contrast injection. The box surrounding the enhancing lesion is the MRS voxel. Corresponding spectra are shown to the right. The spectral peaks in figure (a) labeled 1-3 arise from lipid, tCho, and water, respectively. The line above and below the tCho peak show the fitted tCho peak and the fitting residual, respectively. (a) baseline study 2 days prior to starting AC, $[tCho]_0$ = 4.6 mmol/kg, LD_0 = 4.0 cm, (b) study at 24 hrs after the first cycle of AC, $[tCho]_{24}$ = 3.7 mmol/kg, LD = 4.0 cm, (c) study after the fourth cycle of AC, [tCho] = 0.9 mmol/kg, LD = 1.7 cm, (d) study after the second cycle of paclitaxel, [tCho] = 4.1 mmol/kg, LD = 1.7 cm. Using equation 4, after the first cycle of AC, $\%\Delta$[tCho] was -20%, predicting an objective response to AC. Using equation 2, after the fourth cycle of AC, $\%\Delta$LD was -58%, compatible with an objective response to AC.

Figure 3 - Relationship between [tCho] and LD in patients with no response. The dashed line represents the normalized baseline value for $[tCho]_0$ and LD_0. The diamonds

represent the calculated $\%[tCho]_{24}$ and the circles represent the calculated $\%LD_f$. $[tCho]_{24}$ and LD_f pairs from individual subjects are indicated by connecting lines. Notice that all the nonresponding patients had a $[tCho]_{24}$ which was greater than or equal to $[tCho]_0$.

Figure 4 – MRI and MRS of a nonresponding patient. Images are sagittal view, right breast, acquired with T1-weighed high resolution 3D FLASH using fat suppression at 7 minutes post contrast injection. The box surrounding the enhancing lesion is the MRS voxel. Corresponding spectra are shown to the right. The spectral peaks in figure (a) labeled 1-3 arise from lipid, tCho, and water, respectively. The line above and below the tCho peak show the fitted tCho peak and the fitting residual, respectively. (a) Baseline study 1 day prior to starting AC, $[tCho]_0 = 1.4$ mmol/kg, $LD_0 = 2.9$ cm, (b) study at 24 hrs after the first cycle of AC, $[tCho]_{24} = 2.1$ mmol/kg, LD = 2.9 cm, (c) study after the fourth cycle of AC, [tCho] = 0.9 mmol/kg, $LD_f = 2.7$ cm. Using equation 4, after the first cycle of AC, $\%\Delta$[tCho] was 50%, predicting no response to AC. Using equation 2, after the fourth cycle of AC, $\%\Delta LD$ was -7%, compatible with a nonresponder to AC.

Figure 5 – Correlation between $\%\Delta$[tCho] and $\%\Delta LD$. Each solid white square represents one of the 8 objective responding patients and each solid black square represent one of the 5 nonresponding patients. There is a statistically significant positive correlation between $\%\Delta$[tCho] and $\%\Delta LD$; ($R = 0.89$, $p < 0.0001$). Notice that all 8 objective responding patients had a $\%\Delta LD$ greater than -30% with a $\%\Delta$[tCho] less than

zero and all 5 nonresponding patients had a %ΔLD less than -30% with %Δ[tCho] greater than or equal to zero.

Table 1

Tumor Size, Total Choline Concentration, Diagnosis, Clinical Response, and Prognostic Factors

Patient No	LD_0 (cm)	LD_f (cm)	$[tCho]_0$ (mmol/kg)	$[tCho]_{24}$ (mmol/kg)	Diagnosis	Clinical Response	ER/PR
1	4.0	1.7	4.6	3.7	IDC/DCIS	OR	+/-
2	6.8	3.3	1.7	0.9	ILC/DCIS	OR	+/-
3	9.3	4.2	7.8	5.4	IBC	OR	-/+
4	2.8	0	2.7	0	IDC/DCIS	OR	+/+
5	3.1	0.8	1.1	0.7	IDC	OR	-/-
6	2.1	1.0	4.5	3.0	ILC/LCIS/DCIS	OR	+/+
7	2.3	0.7	1.4	1.1	IDC/DCIS	OR	-/+
8	4.8	3.1	8.5	6.1	IDC/DCIS	OR	+/-
9	9.5	9.5	1.1	1.1	IBC/DCIS	NR	-/-
10	2.9	2.7	1.4	2.1	IDC	NR	-/-
11	3.8	3.3	1.0	1.1	IDC/ILC	NR	+/+
12	6.8	6.1	1.5	1.9	IBC/LCIS	NR	+/-
13	3.2	3.4	2.3	3.4	IBC	NR	+/-

LD_0 = tumor size at baseline, LD_f = tumor size after final dose of AC, $[tCho]_0$ = total choline concentration at baseline, $[tCho]_{24}$ = total choline concentration within 24 hours after the first cycle of AC, ER = estrogen receptor, PR = progesterone receptor, IDC = invasive ductal carcinoma, ILC = invasive lobular carcinoma, IBC = inflammatory breast cancer, DCIS = ductal carcinoma in situ, LCIS = lobular carcinoma in situ, OR = objective response, NR = no response, + = positive, - = negative

Figure 1

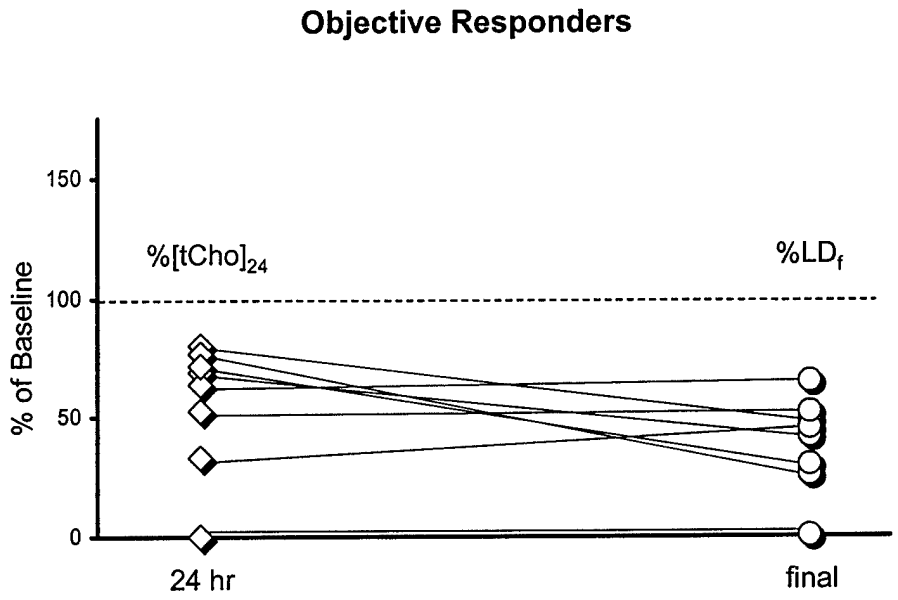
Objective Responders
150
100
50
0
% of Baseline
%[tCho]24
%LDf
24 hr
final

Figure 2

Objective Responding Patient

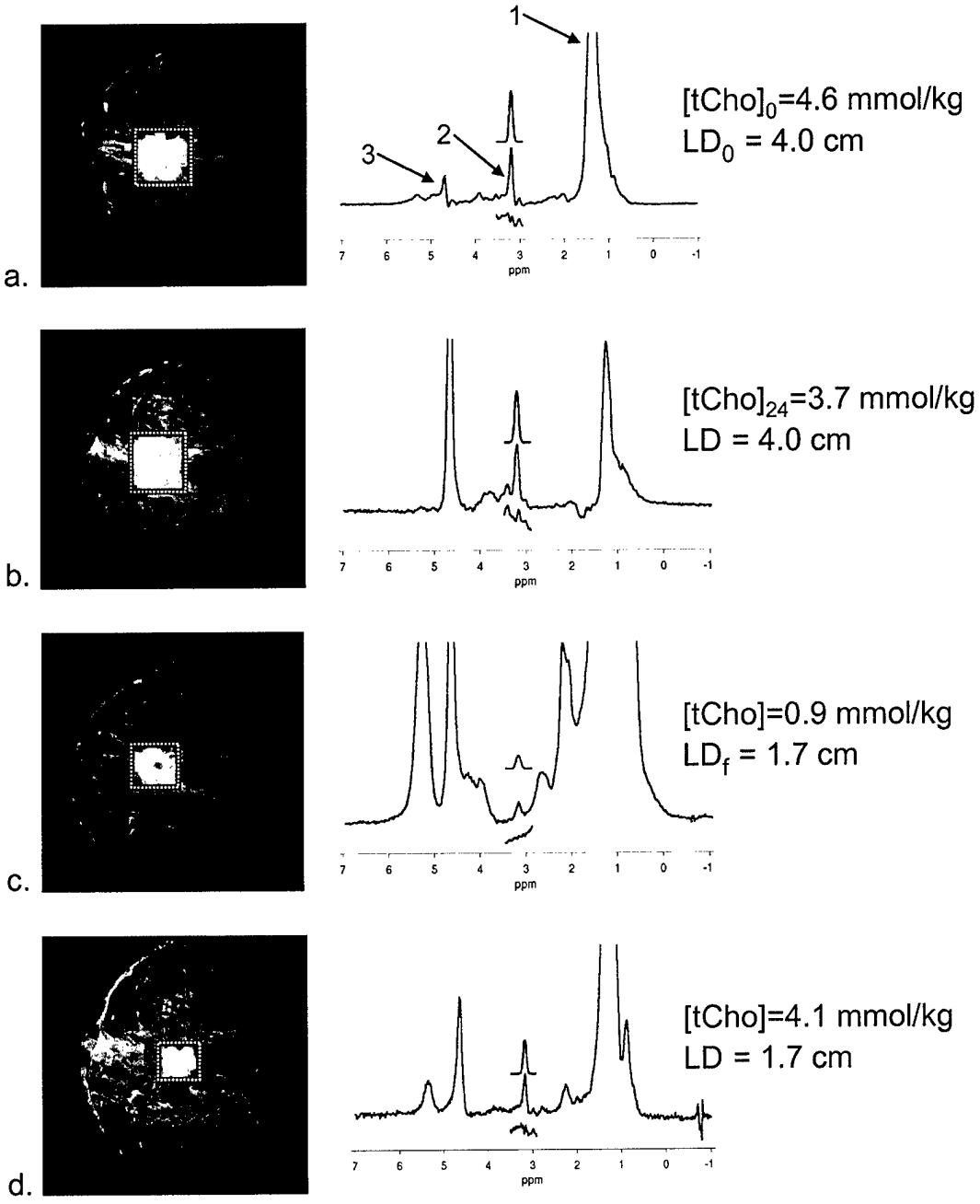

%Δ[tCho] = -20%, %ΔLD = -58%

Figure 3

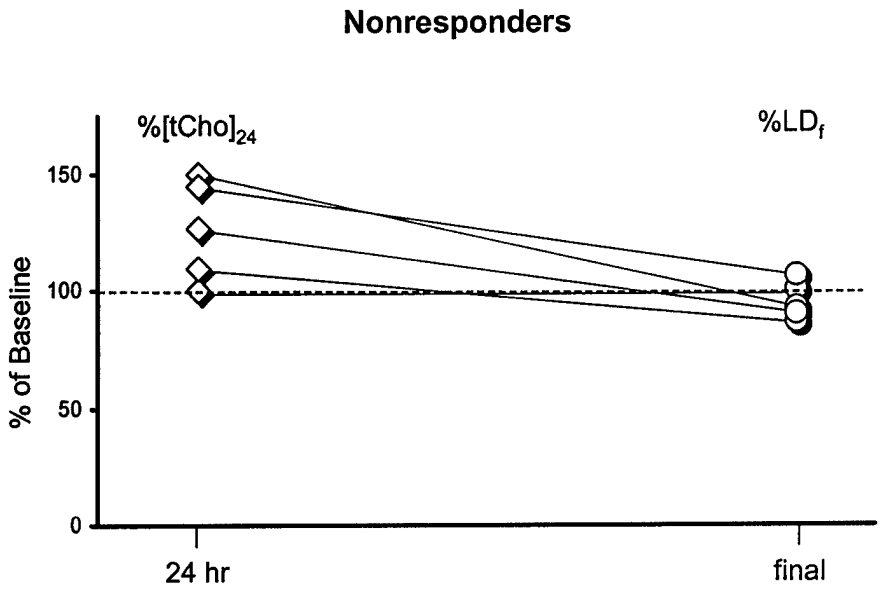
Nonresponders
%[tCho]24
%LDf
150
100
50
0
% of Baseline
24 hr
final

Figure 4

Nonresponding Patient

a.

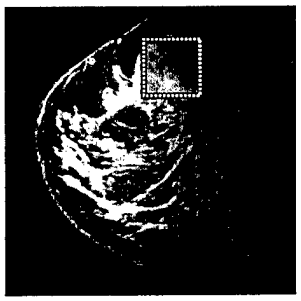

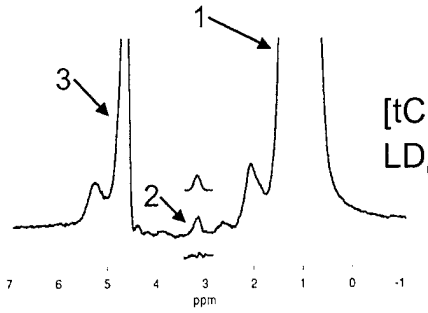

$[tCho]_0$=1.4 mmol/kg
LD_0 = 2.9 cm

b.

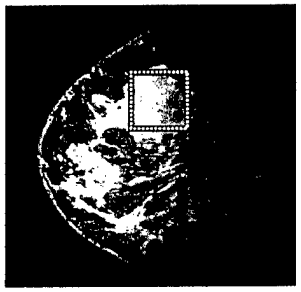

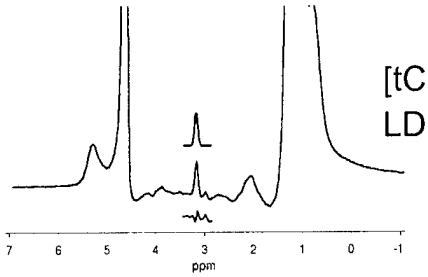

$[tCho]_{24}$=2.1 mmol/kg
LD = 2.9 cm

c.

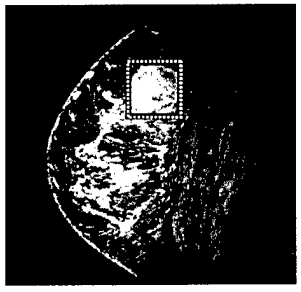

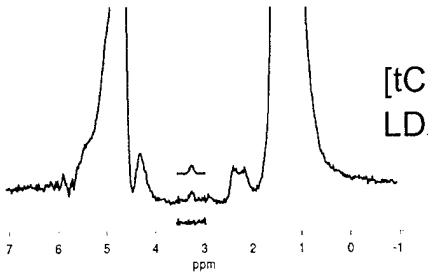

[tCho] =0.9 mmol/kg
LD_f = 2.7 cm

%Δ[tCho] = 50%, %ΔLD = -7%

Figure 5

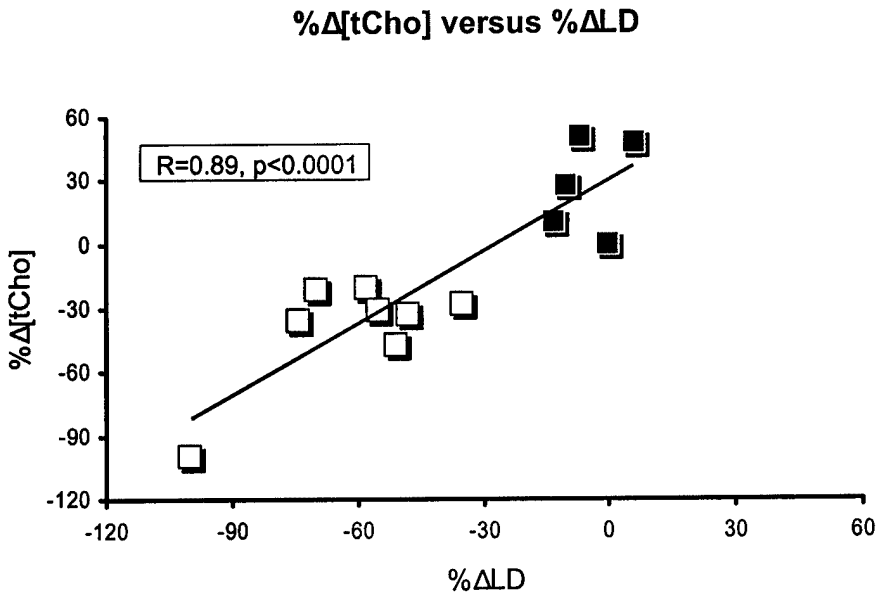
%Δ[tCho] versus %ΔLD
R=0.89, p<0.0001
%Δ[tCho]
60
30
0
-30
-60
-90
-120
-120
-90
-60
-30
0
30
60
%ΔLD

In Vivo Quantification of Choline Compounds in the Breast with ^{1}H MR Spectroscopy

Patrick J. Bolan[1,2], Sina Meisamy[1,2], Eva H. Baker[1,2], Joseph Lin[1,2], Timothy Emory[2], Michael Nelson[2], Lenore I. Everson[2], Douglas Yee[3,4], Michael Garwood[1,2,3*]

[1]Center for Magnetic Resonance Research, [2]Department of Radiology, [3]Cancer Center, and [4]Department of Medicine, University of Minnesota School of Medicine, Minneapolis, Minnesota

* Correspondence to: Michael Garwood, Ph.D., Center for Magnetic Resonance Research, 2021 Sixth Street SE, Minneapolis, MN 55455. Email: gar@cmrr.umn.edu

Presented in part at the ISMRM Workshop on *In Vivo* Functional and Molecular Assessment of Cancer, Santa Cruz, CA, October 19-21, 2002, for which the first author received the Negendank Award.

Grant Sponsors:
NIH Grants RR08079, CA92004, RR00400, CA77398
DOD Breast Cancer Research program DAMD 17-01-1-0331
Tickle Family Land Grant Endowment in Breast Cancer Research

Word Count: Abstract 150; Body 5586; Total 7484

Running Head: Quantification of tCho in Breast

Abstract

This work describes a methodology for quantifying levels of total choline-containing compounds (tCho) in the breast using *in vivo* ^{1}H MR spectroscopy at high field (4 Tesla). Water is used as an internal reference compound to account for the partial volume of adipose tissue. Peak amplitudes are estimated by fitting one peak at a time over a narrow frequency band to allow measurement of small metabolite resonances in spectra with large lipid peaks. This quantitative method represents a significant improvement over previously reported analysis methods by accounting for the variable sensitivity of breast ^{1}H MRS measurements. Using this technique, a tCho peak could be detected and quantified in 214 of 500 *in vivo* spectra. Levels of tCho were found to be significantly higher in malignancies than in benign abnormalities and normal breast tissues, suggesting that this technique could be used for diagnosing suspicious lesions and monitoring response to cancer treatments.

Key words

choline; breast cancer; quantification; MRS

Introduction

Breast cancer is a very common disease, affecting 11% of American women in their lifetimes and causing more than 40,000 deaths each year (*1*). While breast cancer mortality is decreasing, incidence continues to rise (*2*). Thus, there is a great need for non-invasive diagnostic tools for both screening and treatment monitoring. The conventional diagnostics – X-ray mammography, sonography, and physical examination – are limited in both their sensitivity for detecting disease and their specificity for distinguishing between benign and malignant lesions. The use of magnetic resonance imaging (MRI) of the breast has been increasing due to its high sensitivity, but its reported specificity is widely variable (*3*).

More recently, researchers have been augmenting breast MRI studies with magnetic resonance spectroscopy (MRS) to increase specificity. *In vivo* MRS can detect a resonance at 3.25 ppm that has contributions from several different compounds, including choline, phosphocholine, glycerophosphocholine, and taurine. High resolution *in vitro* and *ex vivo* studies indicate that the levels of choline compounds increase with malignancy (*4-6*). At lower field strengths used for *in vivo* work (1.5-4 T), these multiple resonances cannot be spectrally resolved and so appear as a single peak, termed total choline-containing compounds (tCho).

Several studies reported at 1.5 T have shown that *in vivo* MRS can be used to distinguish between benign and malignant tissues (*7-11*). These studies used the hypothesis that tCho is only detectable in malignancies. A pooled analysis of these five studies showed that this tCho detectability criterion can identify malignancies with an 83% sensitivity and 85% specificity (*12*). This qualitative approach is promising, but it is only applicable if the MRS measurement sensitivity is invariant. In similar studies performed at 4 T, the increased sensitivity allows detection of tCho in benign lesions and in normal subjects. A more general approach is to

quantify the tCho peak with the expectation that tCho levels are higher in malignancies than in benign lesions or normal tissues. Two groups have reported quantification of tCho levels using external phantom referencing methods (*7, 13*). These studies demonstrated the feasibility of quantitative breast MRS, but they were limited to small patient groups and they did not report measurement errors. Quantification is also valuable for measuring tumor response to treatment regimens. Two studies have reported that the detectability and amplitude (judged qualitatively) of the tCho peak decreases after chemotherapy (*8, 11*). A quantitative method enables finer measurements of the magnitude and rate of tumor response.

Although quantification of metabolite levels is routinely performed in MRS of the brain, it is more difficult to perform in the breast due to the heterogeneous distribution of the glandular and adipose tissues. Although the spectroscopist will typically plan a voxel to include mainly glandular tissue and tumor, voxels of typical size (1-2 mL) nearly always contain some adipose tissue as well. The amount of included adipose tissue can vary greatly depending on the architecture of the gland and/or lesion.

The two basic elements of a quantitative MRS methodology are the referencing strategy and the spectral fitting technique. The referencing strategy proposed in this paper uses water as an internal reference peak. This approach compensates for the partial volume of adipose tissue in the voxel and naturally leads to a molal (mol/kg) concentration for water soluble metabolites. The fitting technique used in this work is based on the TDFD approach (*14*). This method allows flexible lineshape definition by using a time domain model, and has excellent frequency-selection properties since the residuals are evaluated and minimized in the frequency domain. The ability to select a narrow frequency range is crucial for fitting small resonances in the presence of very large ones, as is the case in breast spectra containing large lipid peaks.

The goal of this project was to develop a method for quantitatively measuring levels of tCho in breast tissue. The methodology presented integrates several existing techniques: single-voxel localization using LASER (*15*), TE averaging to reduce lipid sideband artifacts (*16*), automatic frequency referencing to correct respiration artifacts, frequency-selective spectral fitting, and quantification using water as an internal reference peak. The results from quantifying 500 *in vivo* spectra with this technique are presented and analyzed, and compared with an independent method based on external referencing. The applicability of using quantitative ^{1}H MRS for diagnosing suspect breast lesions is discussed.

Methods

Acquisition

All measurements were performed with a hybrid 4 T system, consisting of a 90 cm bore magnet (model 4 T-900, Oxford Magnet Technology, Oxfordshire, UK) with a clinical gradient system (model *Sonata*, Siemens, Erlangen, Germany) interfaced with an imaging spectrometer (model *Unity Inova*, Varian, Palo Alto, CA). Several different single-breast quadrature transmit/receive RF surface coils of similar design were used to accommodate different breast sizes. The coils were mounted onto a custom-built patient table designed for unilateral, prone breast studies.

A total of 105 subjects (ages 23-72, mean 48) were studied in 175 MRI/MRS sessions. Of these, 86 were participants in a study for diagnosing lesions with suspicious mammographic findings, 14 were participants in a study for monitoring response to neoadjuvant chemotherapy, and 5 were presumed normal volunteers (no breast-related health problems or abnormal mammograms). Approximately half of these studies were performed after a needle biopsy or

other invasive procedure. All studies were approved by the institutional review board. Informed written consent was obtained prior to all studies.

All 100 patients from the diagnosis and treatment monitoring studies were examined with the same MRI/MRS protocol consisting of high-resolution imaging, dynamic contrast-enhanced imaging, and single-voxel spectroscopy. Subjects were positioned prone with their breast centered horizontally in the magnet. After acquiring scout images to verify position, the coil was manually tuned and matched. A high-resolution 3D FLASH image (fat-suppressed, matrix = 256 x 256 x 64, field of view = 14-18 cm, TE/TR = 4.1/13.5 ms, flip angle = 30°) and a fast 2D multislice image (fat-suppressed, matrix = 256 x 128, 30 slices, slice thickness = 2.5 mm, field of view = 14-18 cm, TE/TR = 5.1/390 ms, flip angle = 90°) were acquired prior to injection of Gd-DTPA (0.1 mmol/kg body weight). Five to seven 2D images were acquired immediately after injection, followed by a second 3D image. Both image sets were analyzed using our own image processing software (developed with Matlab; The Mathworks, Natick, MA) to select voxels for MRS with the subject still in the magnet. Criteria for voxel selection included lesion architecture, dynamic Gd-DTPA uptake, and prior clinical knowledge from mammographic or ultrasound images. Voxels were planned to maximize coverage of the lesion while minimizing the inclusion of adipose tissue. The 5 normal subjects were studied with only the high-resolution 3D FLASH image followed by spectroscopy, since no Gd-DTPA was administered in these studies.

All spectra were acquired using the LASER localization technique (*15*) with 4096 complex points and 6 kHz spectral width. Each voxel measurement began with a calibration of the localized B_1 field strength, followed by 30-60 s of manual adjustment of the linear shims. A fully relaxed, single-shot, unsuppressed spectrum was acquired to measure the water and lipid peaks. The power required to suppress the water signal using VAPOR (*17*) suppression was then

manually adjusted. The metabolite spectrum was acquired using TE averaging with TE = 45-196 ms in 64 or 128 increments and with TR=3 s (*16*). Each free induction decay signal (FID) was individually saved – no averaging was performed until processing. Each voxel required ~9 minutes in total. Typically 1-4 voxels were studied in each subject for a total acquisition time of ~1 hour.

Pre-processing Spectra

All spectral processing programs, including preprocessing, fitting, and quantification, were written in Matlab (Mathworks, Natick, MA). In all spectra, the last 512 points of the raw time domain FID were used to calculate the root-mean-square noise and to correct for DC offsets. For the unsuppressed spectra used to measure the water and lipid peaks, the FIDs were truncated to 1024 points and then zero-filled to 2048 points. The zero-order phase ϕ was measured and corrected using the average of two different autophasing methods: 1) fitting the phase of the first few time-domain points to a line and using ϕ at time t=0, and 2) finding the value ofϕ which maximizes the smallest value of the real part of the frequency-domain spectrum. Using the mean of these two methods produces a robust estimate of ϕ. The spectra were then frequency referenced by setting the maximum of the water peak to 4.7 ppm. For the water-suppressed spectra used to measure the metabolites, each individual spectrum from the TE averaging acquisition was automatically phased as described above. To correct respiration-induced frequency shifts, each spectrum was shifted in frequency to maximize the cross-correlation function between it and the first spectrum of the acquisition (*18*). After phasing and frequency correction the spectra were averaged.

Fitting

To fit the water, 1.3 ppm lipid, and tCho peaks in the processed spectra, a new fitting program was developed. The algorithm is based on the TDFD (time-domain / frequency-domain) fitting technique proposed by Slotboom *et al.* (*14*). In this approach, a time-domain model is used to describe the peak parameters, but the fitting is performed by applying a Fourier transform and minimizing the residuals in the frequency domain. This flexible fitting method has excellent frequency-selective properties and can be used with various lineshape definitions. In this implementation, a Voigt lineshape was used to model all peaks (*19*). The modeled signal from a single peak s can be described in the time domain t as

$$s(t) = A \cdot \exp(-i\omega t + i\phi - \lambda t - \gamma^2 t^2) \qquad [1]$$

with signal amplitude A, chemical shift frequency ω, zero-order phase ϕ, Lorentzian damping factor λ, and Gaussian damping factor γ. The Lorentzian and Gaussian damping factors are related to the full width at half maximum (FWHM) of an impulse response: $\lambda = \pi \cdot FWHM$ and $\gamma = \pi \cdot FWHM / (2\sqrt{\ln 2})$, as described in Ogg *et al.* (*20*). Note that although all equations in this section are shown with continuous time and frequency for clarity, all calculations were performed with discrete variables.

All peaks were fit one at a time by minimizing the frequency domain residuals over a 0.4 ppm (68 Hz) section of the spectrum centered on the peak. The zero-order phaseϕ was fixed at zero (since it was presumably corrected during preprocessing) and only the real portion of the residual was minimized. Initial values for parameters were generated based on prior knowledge and simple heuristics (*e.g.*, the initial frequency is that of the maximum of the absolute value spectrum over the fitting region). The nonlinear minimization of the residuals was performed

using the optimization toolkit provided with Matlab (function *lsqnonlin*, using the large-scale model option).

In the unsuppressed spectra, water was fit at 4.7 ppm and the polymethylene lipid peak was fit at 1.3 ppm. In the suppressed and averaged spectra, tCho was fit at 3.25 ppm. The baseline around 3.25 ppm is often distorted, so a linear baseline model was used to reduce bias. Figure 1 shows the relationship between the data (S_{data}), model (S_{model}), baseline (S_{baseline}), and residual (R). Using a linear baseline, the residual function to be minimized is

$$R(\omega) = \left[S_{\text{data}}(\omega) - S_{\text{baseline}}(\omega) - FFT\{s_{\text{model}}(t)\}\right]_{\omega_0+0.2\text{ppm}}^{\omega_0-0.2\text{ppm}} \qquad [2]$$

where ω_0 is the center of the frequency range being fit. No baseline correction was used for fitting the water and lipid peaks, so in those cases $S_{\text{baseline}} = 0$ for all ω.

The peak amplitude A is the parameter of greatest interest since it is proportional to the number of nuclei in the voxel. The fitting error was estimated using the Cramer Rao Minimum Variance Bound (CRMVB) of the parameter A:

$$CRMVB_{\text{A}} = \frac{\sigma_{\text{noise}}^2}{\int_{\omega_0+0.2\text{ppm}}^{\omega_0-0.2\text{ppm}} \frac{\partial}{\partial A}\left[FFT\{s_{\text{model}}(t)\}\right] d\omega} \qquad [3]$$

where σ_{noise}^2 is the variance of white, Gaussian noise. The $CRMVB_{\text{A}}$ is not actually an estimate of the fitting error, rather it is a theoretical minimum limit for the estimation accuracy. Nevertheless the $CRMVB_{\text{A}}$ is commonly used in NMR applications for estimating fitting errors (*21*). Effectively, this measure is the noise variance scaled by the sensitivity of the model to changes

in the parameter A. The error is often expressed as a normalized standard deviation:

$\sigma_A = \sqrt{CRMVB_A} / A$.

This error estimate was also used to establish the detection criteria. In all cases, a fit was initially performed and the parameter estimates and errors were calculated. If the fitting error for A was greater then a specified threshold, then the fit was rejected and the resonance was considered undetectable. For all spectra reported in this paper the threshold for the normalized error was unity: if $\sigma_A > 1$ the peak was considered undetectable. Although statistically arbitrary, this threshold is convenient and roughly corresponds to a signal-to-noise ratio of 2-3.

Quantification

The spectral fitting produces an amplitude A for each peak, expressed in arbitrary units (au). To standardize this measurement for use in both internal and external referencing schemes, several corrections must be made to account for experimental conditions and the physical properties of each species. The corrected amplitude A' is:

$$A' = \frac{A}{f_{\text{gain}} f_{\text{coil}} f_{T_1} f_{T_2}} \quad [4]$$

with correction factors

$$f_{\text{gain}} = gain / gain_0 \quad [5]$$

$$f_{\text{coil}} = B_1 / B_{1,0} \quad [6]$$

$$f_{T_1} \approx 1 - \exp(-TR / T_1) \quad [7]$$

$$f_{T_2} = \frac{1}{N}\sum_{j=1}^{N} \exp(-TE_j / T_2), \qquad [8]$$

where *gain* is the receiver gain, B_1 is the local amplitude of the excitation radiofrequency field, *TR* is the pulse repetition time, and *TE* is the echo time. The receiver correction factor f_{gain} is necessary if the receiver gain is different in the suppressed and unsuppressed acquisitions. The coil receive efficiency factor f_{coil} was calculated by assuming the transmit and receive efficiencies are equal. The reference values $gain_0$ and $B_{1,0}$ are arbitrary but must be used consistently when comparing values from different acquisitions. The T_1 correction f_{T_1} is approximate, and is valid provided *TR*>>*TE*. With a TE averaged acquisition, the T_2 correction f_{T_2} is a summation over N acquisitions, each with different a TE (*16*). Because it is impractical to measure relaxation properties in each voxel, constant values were assumed for all relaxation constants based on measurements in several subjects.

After these corrections, the signal amplitudes are proportional to the number of nuclei in the volume. The ratio of the tCho and water amplitudes can be converted to molal concentration (moles solute per mass solvent) by correcting for the number of ^{1}H nuclei per molecule η and the molecular weight of the solvent MW_{water}:

$$[\text{tCho}] = \left(\frac{A}{f_{gain} f_{T_1} f_{T_2}}\right)_{tCho} \left(\frac{f_{gain} f_{T_1} f_{T_2}}{A}\right)_{water} \frac{\eta_{water}}{\eta_{tCho} MW_{water}} \qquad [9]$$

Note that the coil efficiency factor f_{coil} cancels because both water and tCho come from the same volume of interest. This quantity [tCho], expressed in units mmol/kg, is the metric proposed as an *in vivo* measure of the tissue level of choline-containing compounds in the breast. This

measurement is presented along with the standard deviation of the fitting error: $[\text{tCho}] \pm [\text{tCho}] \cdot \sigma_A$.

In spectra where no tCho peak was detected based on the $\sigma_A > 1$ criterion, an additional procedure was performed to determine the sensitivity of the measurement. A simulated, noiseless spectrum containing a single peak at 3.25 ppm with a Gaussian FWHM of 15 Hz and amplitude A_{sim} was added to the preprocessed *in vivo* spectrum. The combined *in vivo* + simulated spectrum was then fit using the procedure described above, and the fitting error σ_A was calculated. This process was repeated with successively smaller simulated peak amplitudes, reduced 10% each iteration, until the simulated peak was no longer detectable. The smallest value of A_{sim} that lead to a detectable tCho peak was then used to calculate a minimum detectable level of tCho, $[\text{tCho}]_{\text{MDL}}$, using Eq. 9. For these *in vivo* spectra where tCho is not detectable, the overall [tCho] measurement is expressed as $0 \pm [\text{tCho}]_{\text{MDL}}$.

To validate this proposed internal referencing scheme, the tCho level was also calculated independently using an external referencing scheme. In general, the corrected signal amplitude A' of a resonance is proportional to the number of nuclei n in the sample: $n = \kappa_{\text{sys}} A'$. The system constant κ_{sys} (with units mol/au) accounts for the system-specific hardware and software. The value of κ_{sys} was calculated for our system in separate calibration experiments with a phantom of known concentration and measurable relaxation properties. The externally-referenced concentration of tCho can then be expressed in molal units (mol/kg) as

$$[\text{tCho}]_{\text{ext}} = \left(\frac{A}{f_{\text{gain}} f_{B_1} f_{T_1} f_{T_2}} \right)_{\text{tCho}} \frac{\kappa_{\text{sys}}}{\eta_{\text{tCho}}} \frac{1}{V \rho_{\text{water}}} \qquad [10]$$

with ρ_{water} as the water density and V as the voxel volume. To compare the internal and external methods, the tissue water density was assumed to be 1 kg/L. The volume V was assumed to be the entire voxel volume, ignoring the effect of partial volume from adipose tissue.

Results

The quantification method was applied to 500 spectra acquired from 105 subjects in 175 MR study sessions. The voxel size ranged from 0.4 to 16 mL, with a median volume of 1.6 mL. A peak near 3.25 ppm was detected in 214 (43%) of the 500 spectra. The processing and fitting processes required ~1 min per spectrum on a typical workstation. After running the fully-automated procedure on all 500 spectra and manually reviewing the results, 6 spectra required reprocessing with manual intervention to adjust phase and/or frequency referencing. Each water, lipid, and tCho peak was fit with a Voigt lineshape, giving both Lorentzian and Gaussian contributions to the linewidth. The median Lorentzian and Gaussian linewidths for the fit water peak were 12 Hz and 13 Hz respectively; the 1.3 ppm lipid peak had 16 Hz and 28 Hz; the tCho peak had 0 Hz and 14 Hz.

To calculate absolute tCho levels, relaxation values were measured in several subjects using standard spectroscopic techniques. Measured values with standard deviations were: $T_{1,water}$ = 870±325 ms, $T_{2,water}$ = 60±7 ms, $T_{1,lipid}$ = 480±100 ms, $T_{2,lipid}$ = 69±12 ms, and $T_{2,tCho}$ = 399±133 ms. $T_{1,tCho}$ was not measured, but was assumed to be the same as $T_{1,water}$. Although some of these standard deviations are large, their overall effect on the [tCho] measurement is relatively small. Using our acquisition parameters, the uncertainties in $T_{1,water}$, $T_{2,water}$, $T_{1,tCho}$, and $T_{2,tCho}$ lead to [tCho] standard deviations of 0, 5, 6, and 13%, respectively, for a total of 16%.

Several examples of *in vivo* spectra are shown in Fig. 2. Figure 2a shows a large voxel acquired in healthy glandular tissue. A clear tCho peak is visible at 3.25 ppm, and the fitting

produces a measurement of [tCho] = 0.75 ±0.07 mmol/kg. The model fit of this peak is shown above the full spectrum, and the smooth residual is shown beneath. There is another metabolite peak visible at 3.4 ppm that was not fit. This sample shows that tCho can be detected in normal breast tissue. Figure 2b is a spectrum from an invasive ductal carcinoma with [tCho] = 6.8±0.09 mmol/kg. The volume of this voxel is smaller than that of the voxel in Fig. 2a, but since it is located closer to the coil the sensitivity is comparable. The signal-to-noise of the tCho peak is quite high but the residual shows some structure, indicating an imperfect fit. Figure 2c shows a more typically-sized voxel in a lesion later identified by needle biopsy as atypical hyperplasia, with [tCho] = 1.5±0.8 mmol/kg. The diagnosis of atypical hyperplasia is generally considered benign but is a marker indicating an increased risk for developing future malignancies. The low SNR of the tCho peak is reflected in the error estimated by the fitting procedure.

These examples demonstrate how the sensitivity of breast MRS can vary greatly. Due to variability in coil loading, voxel size, and partial volume of adipose tissue, the sensitivity for detecting tCho varied by a factor of greater than 100 in this study. Figure 3 shows the fitting error in all 500 spectra as a function of a) water SNR and b) voxel volume. For both natural and simulated spectra, the fitting error is the normalized error multiplied by the calculated concentration, $[\text{tCho}]\cdot\sigma_A$ or $[\text{tCho}]_{MDL}\cdot\sigma_A$. Clearly the water SNR is a better indicator of fitting error, since it automatically corrects for coil efficiency and the partial volume of adipose tissue. These plots show reasonable properties for an unbiased fitting method. For example, fitting error decreases uniformly with increasing water SNR, and tCho is more likely to be detected in spectra with lower fitting errors.

Although the fitting error is greater in smaller voxels, the [tCho] measurement itself is independent of the voxel size, as shown in Fig. 4a. The filled diamonds represent [tCho]

measurements in spectra where a peak was detectable; hollow diamonds represent the minimum detectable level of tCho in spectra where no peak was detectable. As expected, smaller voxels are less likely to have detectable tCho, but clearly the voxel size did not bias the [tCho] measurement in spectra with detectable tCho.

Figure 4b shows how the [tCho] measurement varies with the lipid content of the voxel. The lipid fraction is estimated using the ratio between the corrected amplitudes of the water and 1.3 ppm lipid peaks: $\text{lipid}\,\% = A'_{\text{lipid}} / (A'_{\text{water}} + A'_{\text{lipid}}) \times 100$. The [tCho] measurement was expected to be independent of the voxel lipid fraction because all the metabolites contributing to the tCho peak are water-soluble. In voxels with low to moderate lipid content, [tCho] was independent of the lipid fraction. In voxels with large lipid content, however, the [tCho] measurement increases with increasing lipid fraction. Lipids apparently contribute to the amplitude of the tCho peak, either through baseline artifacts not suppressed by TE averaging or by a true resonance at 3.25 ppm. Due to this lipid contamination, we arbitrarily chose a cutoff value of 33%, above which the [tCho] measurement is considered biased and the MRS measurement is considered invalid.

Figure 5 shows a comparison between the internal and external reference schemes described in Methods. This shows that in good quality spectra, where tCho is detectable and the lipid content is low, both internal and external methods produce consistent results ($R^2 = 0.91$). The absolute values produced by the external method are lower, due to overestimation of the product $(V \cdot \rho_{water})$ in the denominator of Eq. 10, which represents the aqueous content of the voxel.

The applicability of the [tCho] measurement for diagnosing different pathologies is shown in Fig. 6. All spectra that had sufficient quality (free of artifacts, lipid fraction = 33%) and were acquired from lesions with biopsy-confirmed pathology were divided into a *malignant*

category (including infiltrative ductal, lobular, and unspecified carcinomas) and a *benign* category (including atypical hyperplasias, fibroadenomas, fibrocystic changes, and cysts). There were insufficient data to distinguish further histological subcategories or tumor staging grades. When multiple spectra were acquired from a single lesion, only the spectrum with the smallest error was included in this chart. Spectra labeled *normal* were acquired from normal volunteers and from regions of normal-appearing and asymptomatic glandular tissue in other subjects. These results show that the tCho measurement is elevated in malignancies and in some benign lesions. The mean [tCho] is greater in malignancy than in benign tissues ($p=0.008$, one-tailed t-test), but the difference between the normal and benign categories is not statistically significant ($p=0.17$). An ROC analysis was performed to determine a threshold [tCho] value for distinguishing between benign and malignant lesions. Using equal weighting for false positives and false negatives, the criteria for malignancy is [tCho] = 1.38 mmol/kg. With this cutoff, the sensitivity is 46% and the specificity is 94%. Note that neither of these analyses take into account the variable sensitivity.

Single-voxel MRS in the breast is very sensitive to the size and placement of the voxel due to the heterogeneous distribution of tCho in the breast, as can be seen in the spectra shown in Fig. 7. All three spectra were acquired from different regions of the same 3 cm tumor, a grade III invasive ductal carcinoma studied after the patient had received four months of chemotherapy. In a large voxel covering most of the tumor, [tCho] was measured to be 1.1±0.6 mmol/kg. The anterior, enhancing portion of the tumor had a higher [tCho] (1.5±0.5 mmol/kg), whereas the posterior, non-enhancing region had no detectable peak ([tCho] = 0±1.3 mmol/kg). The sensitivity is lowest in the posterior voxel due to its distance from the coil, small voxel size, and higher lipid content. This example underscores the importance of proper voxel placement.

Discussion

This work describes a new method for quantifying the levels of total choline-containing compounds (tCho) in breast tissues. Quantitative MRS is a substantial improvement in methodology over the qualitative detection methods used in previous published reports of breast MRS. Quantification is particularly important in the breast because the sensitivity of the MRS measurement is generally more variable than in brain tissue, primarily due to highly variable adipose tissue content and greater variation of the coil receive efficiency. Previous *in vivo* studies have used the hypothesis that detectability of tCho is associated with malignancy, but this approach is only valid if the detection threshold is constant. We have found that using a higher B_0 field (4 T) and optimized surface coils increases the sensitivity enough to enable the detection of tCho in normal breast tissue and several benign lesions.

Two previous reports used external referencing to quantify choline levels in breast tissue (*7, 13*). Neither of these studies corrected for partial volume of adipose tissue within the voxel. In our experience the amount of intravoxel adipose tissue can vary greatly, as shown in Fig. 4b. The breast can be coarsely approximated by a two-compartment model consisting of aqueous regions (fibroglandular tissue) and aliphatic regions (adipose tissue). The aqueous compartment contains all the choline-containing compounds that are known to be elevated in malignancies. Any externally-referenced method must account for this compartmentation to avoid systematic error, whereas an internally-referenced method compensates for compartmentation automatically. Internal referencing methods have further advantages in that they do not require separate calibration experiments, and they use fewer error-introducing correction factors for coil loading, coil efficiency, and voxel volume.

The disadvantage of the internal referencing approach is that it requires the density of NMR-visible water in the aqueous compartment to be relatively constant. There are physiological conditions that affect the water content, but these effects are expected to be small compared to the variability of compartmentation. Both internal and external approaches will be affected by the presence of edema from previous invasive procedures or radiation therapy and by variations in cellularity and relaxation rates. Previous reports expressed concern that the relaxivity of gadolinium contrast agents would deleteriously affect MRS measurements (*8*). In our experience, gadolinium effects are small (~10%) compared to the measurement errors and the variability of tCho levels (*22*).

The spectral fitting software used in this work is highly specialized for fitting peaks in breast spectra, and is available from the authors by request. The method is based on the TDFD technique, which uses an analytical time domain model but minimizes residuals in the frequency domain (*14*). This technique was modified by adding a linear baseline correction and using a very narrow frequency band (0.4 ppm) to fit a single peak at a time. By using only the real component of the spectrum, along with the narrow frequency band and the linear baseline correction, small tCho peaks can be fit without bias from large neighboring lipid resonances.

Another useful feature of the TDFD method is that it permits the use of the Voigt lineshape, which can fit purely Lorentzian or purely Gaussian lineshapes, or any combination of the two. This flexibility was useful for this application because using a Lorentzian or Gaussian model alone did not produce good quality fits for all peaks. The tCho peak is difficult to model precisely because it is a superposition of several resonances, and at 4 T there is not sufficient spectral resolution to separate the individual components. Also, imperfect correction of respiration-induced frequency shifts can cause "blurring" that leads to Gaussian lineshapes in

averaged spectra. Although the Voigt model did not always produce an ideal fit (*e.g.*, Fig 2b) it performed reasonably well in most cases.

The TDFD method was chosen because it is well-suited to the problem and is relatively easy to implement. However, there are numerous other methods that could be adapted for fitting breast spectra. Most other methods are either incapable of fitting a precise frequency range or unable to analytically model a non-Lorentzian lineshape (*23, 24*). The LC Model method (*25*) is very useful for fitting brain spectra, and it could possibly be used for fitting breast spectra. With the currently available implementation of the LC Model software, we were unable to get good quality fits of small tCho peaks in spectra with large lipids. The LC Model method offers some advantages if it could be adapted for breast spectra: it may produce more accurate fits due to its sophisticated baseline model, and it may allow fitting of other metabolites that are occasionally observable in breast spectra, such as creatine, glycine, lactose, and taurine. Automated fitting methods are generally desirable in that they eliminate user interaction and provide a well-accepted measure of error (Cramer-Rao bounds) unbiased by peak lineshape. However, a simple analysis using peak integration and linear baseline correction over manually-defined extents gave comparable results (data not shown).

Cramer Rao Minimum Variance Bounds (CRMVB) are commonly used to estimate the variance of model parameters when fitting NMR spectra (*21*). In this work, the fitting error is used as an estimate of the overall measurement error, although it is probably an underestimate. Most notably, the CRMVB errors from fitting the water are very small, but the actual error in estimating the water amplitude is higher. This occurs because the Cramer Rao theory assumes that the data is perfectly described by the model function, and this assumption is violated by irregular water lineshapes and the overlapping 5.4 ppm lipid resonance. Additionally, there are

experimental factors that can make the true measurement error greater than the fitting error, such as patient motion and respiration. The true measurement error can only be established through repeatability studies. Nevertheless, some estimate of the measurement error is essential for any quantification scheme, and it should be incorporated into the interpretation of quantitative MRS results. It is particularly important in breast MRS because of the highly variable sensitivity, as demonstrated in Fig. 3a. Note that this sensitivity can be estimated prior to acquiring an entire spectrum by using the SNR of the water peak in a single-shot, unsuppressed spectrum. This knowledge can be used to pre-screen voxels for a diagnostic study.

The iterative *minimum detectable level* (MDL) method described here (in which a simulated tCho peak is added to a spectrum and fit) can be used to measure the sensitivity in spectra with no detectable tCho peak. This is critical in interpreting whether a negative finding of tCho is due to lack of sensitivity or low tCho levels. The MDL is closely related to the fitting error: under ideal conditions, the fitting error is equal to the MDL, but in practice the MDL is often larger.

Using a quantitative method for measuring tCho levels in the breast increases the usefulness of MRS for diagnosing benign and malignant lesions. Figure 6 shows [tCho] measurements divided into three broad pathological categories. The finding that tCho levels are higher in malignancies than in benign or normal tissues is consistent with previously published reports that used the detection of tCho to indicate malignancy (*7-11*). The [tCho] threshold of 1.38 mmol/kg, based on an ROC analysis, can be used for distinguishing malignant and benign lesions, but the sensitivity is poor (46%). More data needs to be acquired to determine if subdividing the malignant and benign categories will improve these results (e.g., in the benign category, the two highest values were atypical hyperplasias). Note also that this ROC analysis is

only a first-order method of interpreting the [tCho] levels. More sophisticated analyses should be used which can account for the measurement errors and [tCho] probability distribution functions.

The absolute tCho levels reported in this work, ranging from 0.4 to 10 mmol/kg, are reasonably consistent with previous *in vivo* estimates. Roebuck *et al.* found choline levels from 0.4 – 5.8 mmol/L, and estimated their detection threshold was 0.2 mmol/L (*7*). Bakken *et al.* reported a single measurement of 2 mmol/L (*13*). Further investigations are required to determine whether the absolute [tCho] values reported here are reproducible on different MR scanners and in other institutions.

Figure 6 shows a large range of [tCho] measurements in known cancers, from 0.5 to greater than 8 mmol/kg. It did not appear that tCho levels were related to different histological types of cancer (*e.g.*, lobular *vs.* ductal), but there was insufficient data to establish statistical significance. The variation in [tCho] was also not explained by complicating factors such as recent biopsy or previous chemotherapy treatments, although some of the spectra in which no tCho was detected were acquired from tumors that had been recently biopsied. The large range in [tCho] measurements may be a natural feature of cancers due to variations in the amount of water, lipids, and stroma within the lesion and adjacent tissues, and due to variations in intracellular tCho levels and neoplastic cell density. Previous chemotherapy, radiation, or invasive procedures may further complicate these issues. Additionally, there are experimental factors that can contribute to inaccuracy in these measurements, most notably patient motion and incorrect voxel positioning. If either the biopsy needle or the MRS voxel is placed in the wrong region there will not be agreement between the [tCho] measurements and the histology. Finally, it should be noted that MRS measurements may be adversely affected by metallic radiographic markers, which are widely used but cannot always be identified in heterogeneous breast tissue.

Conclusion

This paper reports a new technique for quantifying levels of total choline-containing compounds (tCho) in breast cancers using single-voxel ^{1}H MRS. Using optimized surface coils and a high field (4 Tesla) scanner, this method was used to measure tCho levels in normal breast tissue and in benign and malignant lesions. Levels of tCho were found to be elevated in malignancies compared to benign lesions, indicating that quantitative MRS may be used to aid in diagnosing breast lesions and monitoring response to cancer treatments.

Acknowledgements

We would like to thank Bibi Husain, Lou Forsythe, R.N., and Julie Gay, R.N. for recruiting and scheduling research subjects, and Robin Bliss, M.S. and Chap Le, Ph.D. for biostatistical consultations.

References

1. Kopans DB. Breast Imaging. 2 ed, Philadelphia: Lippincott-Raven; 1998. 875 p.
2. Howe HL, Wingo PA, Thun MJ, Ries LA, Rosenberg HM, Feigal EG, Edwards BK. Annual report to the nation on the status of cancer (1973 through 1998), featuring cancers with recent increasing trends. J Natl Cancer Inst 2001;93(11):824-842.
3. Orel SG, Schnall MD. MR imaging of the breast for the detection, diagnosis, and staging of breast cancer. Radiology 2001;220(1):13-30.
4. Mackinnon WB, Barry PA, Malycha PL, Gillett DJ, Russell P, Lean CL, Doran ST, Barraclough BH, Bilous M, Mountford CE. Fine-needle biopsy specimens of benign breast lesions distinguished from invasive cancer ex vivo with proton MR spectroscopy. Radiology 1997;204:661-666.
5. Gribbestad IS, Sitter B, Lundgren S, Krane J, Axelson D. Metabolite composition in breast tumors examined by proton nuclear magnetic resonance spectroscopy. Anticancer Res 1999;19:1737-1746.
6. Aboagye EO, Bhujwalla ZM. Malignant transformation alters membrane choline phospholipid metabolism of human mammary epithelial cells. Cancer Res 1999;59(1):80-84.
7. Roebuck JR, Cecil KM, Schnall MD, Lenkinski RE. Human breast lesions: characterization with proton MR spectroscopy. Radiology 1998;209:269-275.
8. Kvistad KA, Bakken IJ, Gribbestad IS, Ehrnholm B, Lundgren S, Fjosne HE, Haraldseth O. Characterization of neoplastic and normal human breast tissues with in vivo 1H MR spectroscopy. J Magn Reson Imaging 1999;10:159-164.

9. Yeung DK, Cheung HS, Tse GM. Human breast lesions: Characterization with contrast-enhanced in vivo proton MR spectroscopy - initial results. Radiology 2001;220:40-46.

10. Cecil KM, Schnall MD, Siegelman ES, Lenkinski RE. The evaluation of human breast lesions with magnetic resonance imaging and proton magnetic resonance spectroscopy. Breast Cancer Res Treat 2001;68(1):45-54.

11. Jagannathan NR, Kumar M, Seenu V, Coshic O, Dwivedi SN, Julka PK, Srivastava A, Rath GK. Evaluation of total choline from in-vivo volume localized proton MR spectroscopy and its response to neoadjuvant chemotherapy in locally advanced breast cancer. Br J Cancer 2001;84(8):1016-1022.

12. Katz-Brull R, Lavin PT, Lenkinski RE. Clinical utility of proton magnetic resonance spectroscopy in characterizing breast lesions. J Natl Cancer Inst 2002;94(16):1197-1203.

13. Bakken IJ, Gribbestad IS, Singstad TE, Kvistad KA. External standard method for the in vivo quantification of choline-containing compounds in breast tumors by proton MR spectroscopy at 1.5 Tesla. Magn Reson Med 2001;46:189-192.

14. Slotboom J, Boesch C, Kreis R. Versatile frequency domain fitting using time domain models and prior knowledge. Magn Reson Med 1998;39(6):899-911.

15. Garwood M, DelaBarre L. The return of the frequency sweep: designing adiabatic pulses for contemporary NMR. J Magn Reson 2001;153(2):155-177.

16. Bolan PJ, DelaBarre L, Baker EH, Merkle H, Everson LI, Yee D, Garwood M. Eliminating Spurious Sidebands in 1-H MRS of Breast Lesions. Magn Reson Med 2002;48(2):215-222.

17. Tkac I, Starcuk Z, Choi IY, Gruetter R. In vivo 1H NMR spectroscopy of rat brain at 1 msec echo time. Magn Reson Med 1999;41:649-656.

18. Henry P-G, van de Moortele P-F, Giacomini E, Nauerth A, Bloch G. Field-frequency locked in vivo proton MRS on a whole-body spectrometer. Magn Reson Med 1999;42(4):636-642.

19. Marshall I, Higinbotham J, Bruce S, Freise A. Use of Voigt lineshape for quantification of in vivo 1H spectra. Magn Reson Med 1997;37(5):651-657.

20. Ogg RJ, Kingsley PB, Taylor JS. The line broadening and unambiguous specification of the Gaussian filter. J Magn Reson A 1995;117:113-114.

21. Cavassila S, Deval S, Huegen C, van Ormondt D, Graveron-Demilly D. Cramer-Rao bounds: an evaluation tool for quantitation. NMR Biomed 2001;14(4):278-283.

22. Bolan PJ, Baker E, DelaBarre L, Merkle H, Yee D, Everson LI, Garwood M. Effects of Gd-DTPA on breast 1H MRS at 4T. In *Proc of 87th Annual Meeting RSNA*. 2001. Chicago.

23. Vanhamme L, Sundin T, Hecke PV, Huffel SV. MR spectroscopy quantitation: a review of time-domain methods. NMR Biomed 2001;14(4):233-246.

24. Mierisova S, Ala-Korpela M. MR spectroscopy quantitation: a review of frequency domain methods. NMR Biomed 2001;14(4):247-259.

25. Provencher SW. Estimation of metabolite concentrations from localized in vivo proton NMR spectra. Magn Reson Med 1993;30(6):672-679.

Figure Captions

Figure 1 – Model showing the frequency-selective fit of a tCho peak with baseline correction. The real component of the raw data is fit with a Voigt lineshape model (thick line) plus a linear baseline (dashed line). The residual (dotted line) is minimized over a 0.4 ppm region centered around the peak. The same model without the linear baseline is used to fit the unsuppressed water and lipid peaks.

Figure 2 – Example spectra. Water-suppressed spectrum is shown on the right, with the tCho fit shown above and the residual (including linear baseline) underneath. The location of the voxel is shown in a contrast-enhanced, fat suppressed sagittal image on the left. A) Normal gland, volume = 13.0 mL, [tCho] = 0.66±0.06 mmol/kg, lipid fraction = 3%; B) Malignant tumor of invasive ductal carcinoma, volume = 6.8 mL, [tCho] = 6.1±0.08 mmol/kg, lipid fraction = 8%; C) Benign finding of atypical hyperplasia in an insensitive region of the coil, volume = 1.1 mL, [tCho] = 1.4±0.7 mmol/kg, lipid fraction = 14%.

Figure 3 – Factors contributing to the sensitivity of [tCho] measurement. Figure 3a shows the fitting error from all 500 spectra as a function of the signal-to-noise ratio of the unsuppressed water peak (time domain amplitude / rms noise). Figure 3b shows the fitting error as a function of total voxel volume. Filled circles are error estimates from spectra where tCho was detectable; open circles are error estimates calculated using the *minimum detectable level* procedure (see text) from spectra where no tCho was detectable.

Figure 4 – Dependence of [tCho] on voxel volume and lipid content. The [tCho] measurement from spectra where tCho was detectable are shown with solid diamonds; for spectra where tCho did not meet the detectability threshold, the minimum detectable levels of tCho are shown with hollow diamonds. Figure 4a shows that the [tCho] measurement is independent of voxel volume, which is desirable. Figure 4b shows that when the lipid volume fraction is low the [tCho] measurement is unbiased. When the lipid content is high the [tCho] measurement increases. Spectra with lipid fractions greater than 33% (an arbitrarily selected threshold) are considered biased.

Figure 5 – A comparison between [tCho] calculated with both internal and external referencing methods in 98 spectra, all with detectable tCho and a lipid fraction = 33%. A linear fit through the origin gives R^2=0.91 and a slope of 0.72. This shows that these measures are highly correlated, although the external method produces somewhat smaller values.

Figure 6 – Measurements of [tCho] in malignant, benign, and normal tissues. Error bars represent standard deviations in spectra where tCho was detectable and minimum detectable levels in spectra where no tCho was detectable. Measurements are ordered from largest to smallest in each category. Malignant and benign spectra were from biopsy-confirmed lesions only. Normal spectra were selected from healthy-appearing glandular tissue with no history of disease.

Figure 7 – Spatial variation of [tCho] measurements within a single tumor. All spectra are from a 3 cm tumor of invasive ductal carcinoma after 4 months of chemotherapy treatment. Images on

the left show voxel positions on a sagittal slice from a contrast-enhanced, fat-suppressed 3D FLASH image. Water-suppressed spectra on the right are shown with the tCho fit above and the residual (including baseline) underneath. In spectrum C) where no tCho was detectable, the minimum detectable level of tCho is shown with a dotted line. A) Voxel containing both enhancing and non-enhancing regions of the tumor, volume = 7.8 mL, [tCho] = 1.1±0.6 mmol/kg, lipid fraction = 5%. B) Voxel acquired from most enhancing region of the tumor, volume = 1.1 mL, [tCho] = 1.5±0.5 mmol/kg, lipid fraction = 2%. C) Voxel acquired from non-enhancing region, volume = 0.9 mL, [tCho] = 0±1.3 mmol/kg, lipid fraction = 13%.

Symbols

s – Italic lower case 'ess'
t – Italic lower case 'tee'
A – Italic upper case 'a'
A_{sim} – Italic upper case 'a', subscript lower case Roman 'sim'
ω, ω_0 – Greek lower case 'omega', subscript 'zero'
ϕ – Greek lower case 'phi'
λ – Greek lower case 'lambda'
γ – Greek lower case 'gamma'
R – Italic upper case 'arr'
S_{data} – Italic upper case 'ess', subscript lower case Roman 'data'
$S_{baseline}$ – Italic upper case 'ess', subscript lower case Roman 'baseline'
S_{model} – Italic upper case 'ess', subscript lower case Roman 'model'
s_{model} – Italic lower case 'ess', subscript lower case Roman 'model'
$CRMVB_A$ – Italic upper case 'cee', 'arr', 'em', 'vee', 'bee', subscript upper case Roman 'a'
σ^2_{noise} – Greek lower case 'sigma', superscript 2, subscript lower case Roman 'noise'
σ_A – Greek lower case 'sigma', subscript upper case Roman 'a'
A' – Italic upper case 'a', superscript 'prime'
A'_{water}, A'_{lipid} – same with subscript lower case Roman 'water' or 'lipid'
f_{gain}, f_{coil} – Italic lower case 'eff', subscript lower case Roman 'gain' or 'coil'
gain, gain$_0$ – Italic lower case 'gain', subscript 'zero'
B_1, B_0 – Italic upper case 'bee', subscript 'one' or 'zero'
$B_{1,0}$ – Italic upper case 'bee', subscript 'one', comma, 'zero'
f_{T_1} – Italic lower case 'eff', subscript upper case Roman 'tee', subscript 'one'
f_{T_2} – Italic lower case 'eff', subscript upper case Roman 'tee', subscript 'two'
N – Italic upper case 'en'
$T_{1,water}$ – Italic upper case 'tee', subscript 'one', comma, 'water'
(plus variations substituting 'two' for 'one', and 'lipid' or 'tCho' for 'water')
$\eta, \eta_{water}, \eta_{tCho}$ – Greek lower case 'eta', subscript lower case Roman 'water' or 'tCho'
MW_{water} – Italic upper case 'em', 'double-U', subscript lower case Roman 'water'
[tCho] – Bracket, Roman lower case 'tee', upper case 'cee', lower case 'h', 'o', end bracket
$[tCho]_{in\ vivo + sim}$ –with subscript lower case Italic 'in vivo', plus symbol, Roman lower case 'sim'
$[tCho]_{ext}$ –with subscript lower case Roman 'ext'
$[tCho]_{MDL}$ –with subscript upper case Roman 'MDL'
n – Italic lower case 'en'
κ_{sys} – Greek lower case 'kappa', subscript lower case Roman 'sys'
ρ_{water} – Greek lower case 'rho', subscript lower case Roman 'water'
V – Italic upper case 'vee'

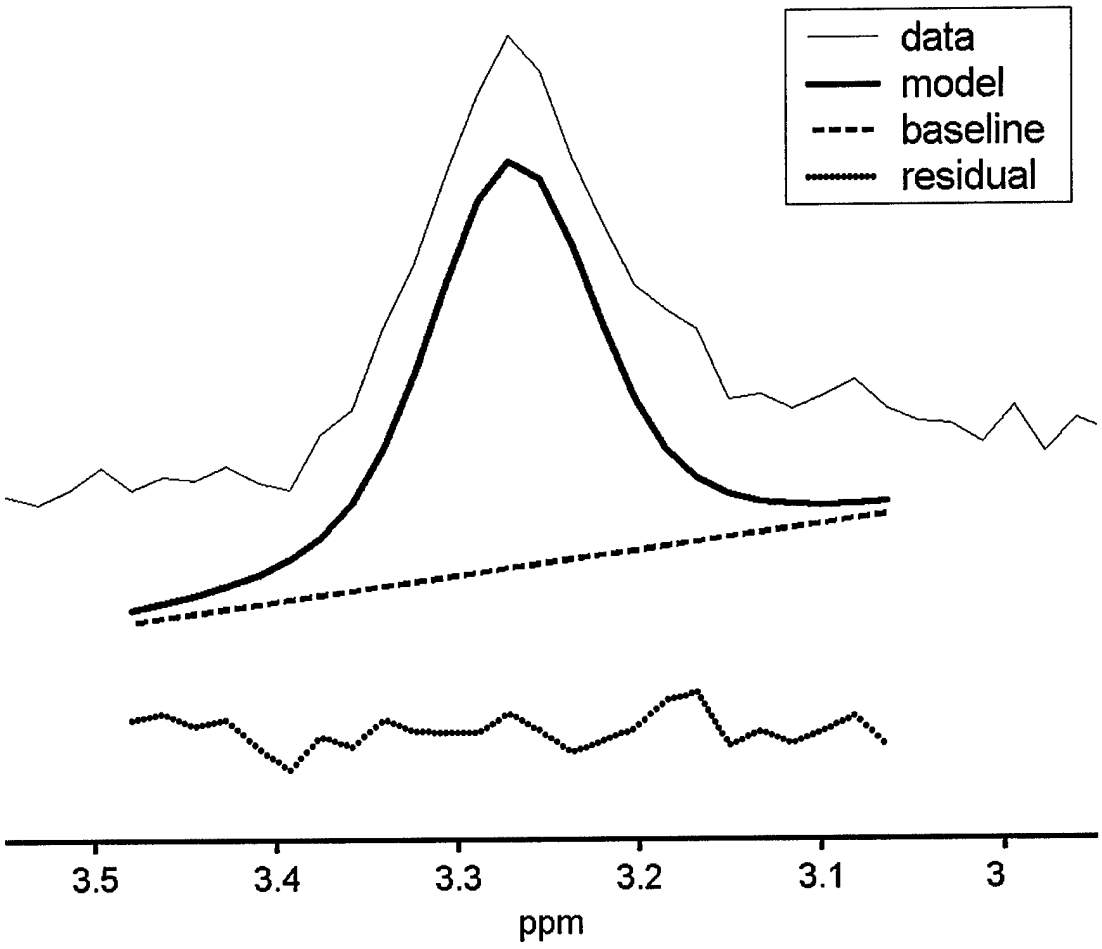

Figure 1

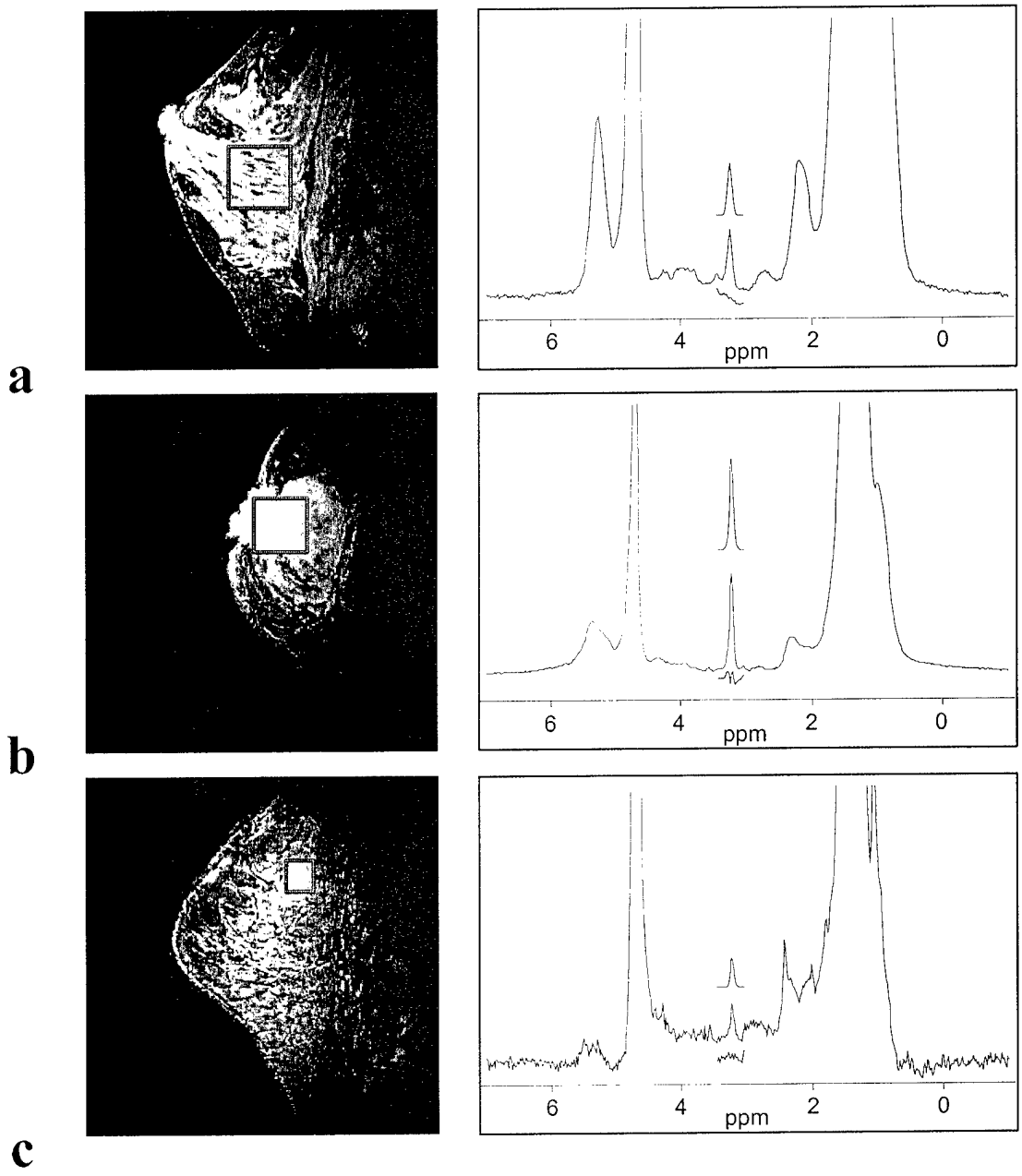

Figure 2

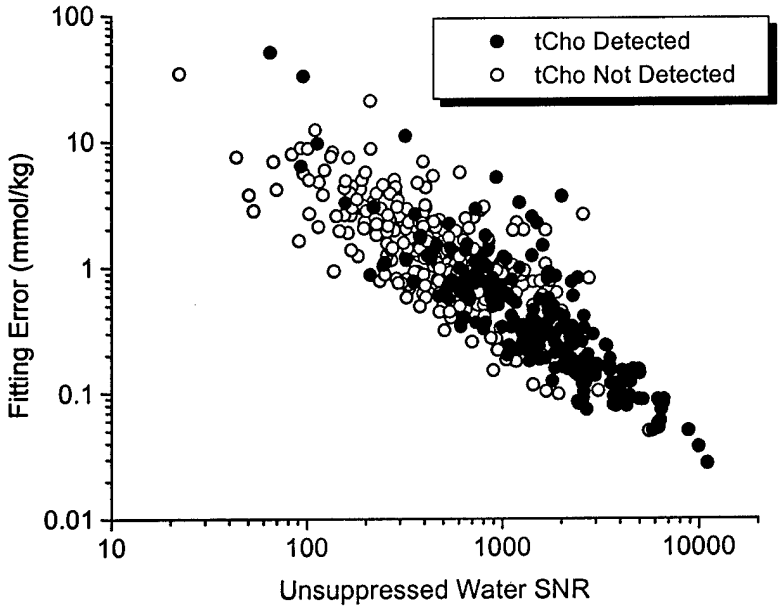
tCho Detected
tCho Not Detected
Fitting Error (mmol/kg)
100
10
1
0.1
0.01
10
100
1000
10000
Unsuppressed Water SNR

a

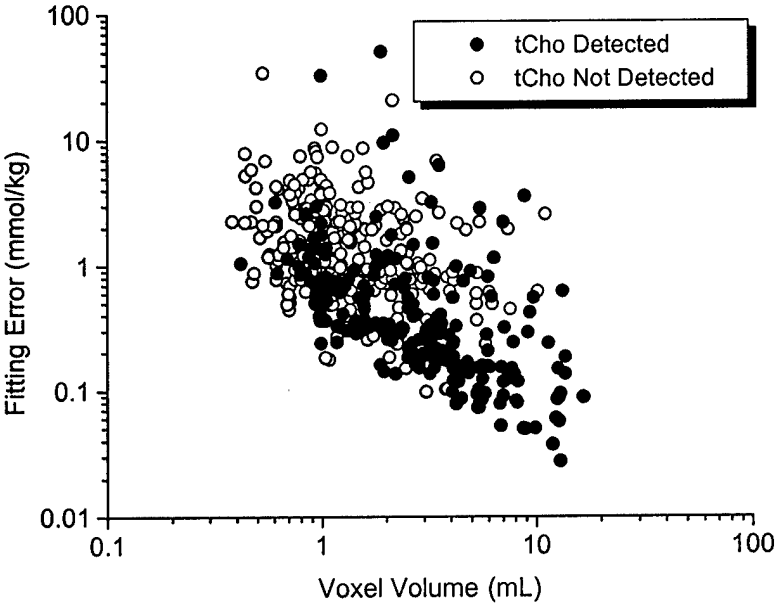
tCho Detected
tCho Not Detected
Fitting Error (mmol/kg)
100
10
1
0.1
0.01
0.1
1
10
100
Voxel Volume (mL)

b

Figure 3

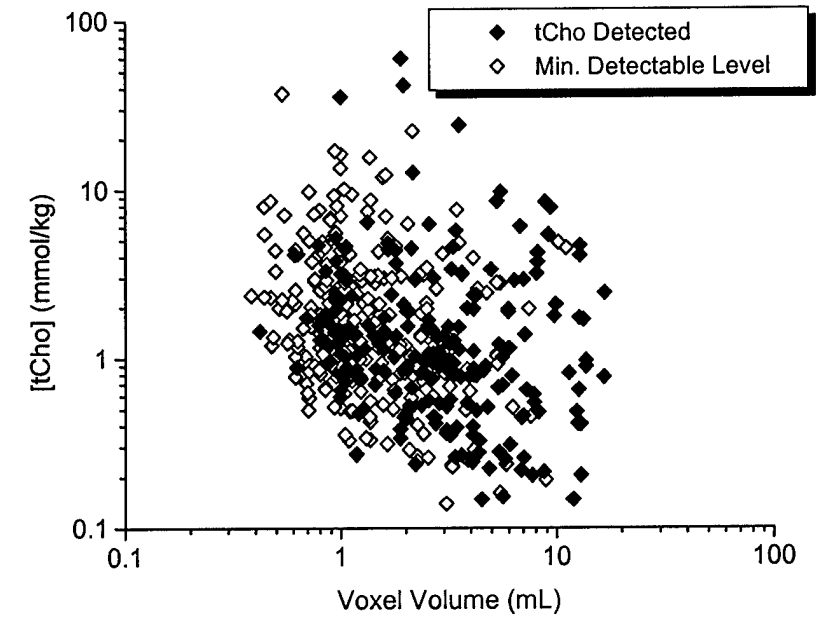
tCho Detected
Min. Detectable Level
[tCho] (mmol/kg)
100
10
1
0.1
0.1
1
10
100
Voxel Volume (mL)

a

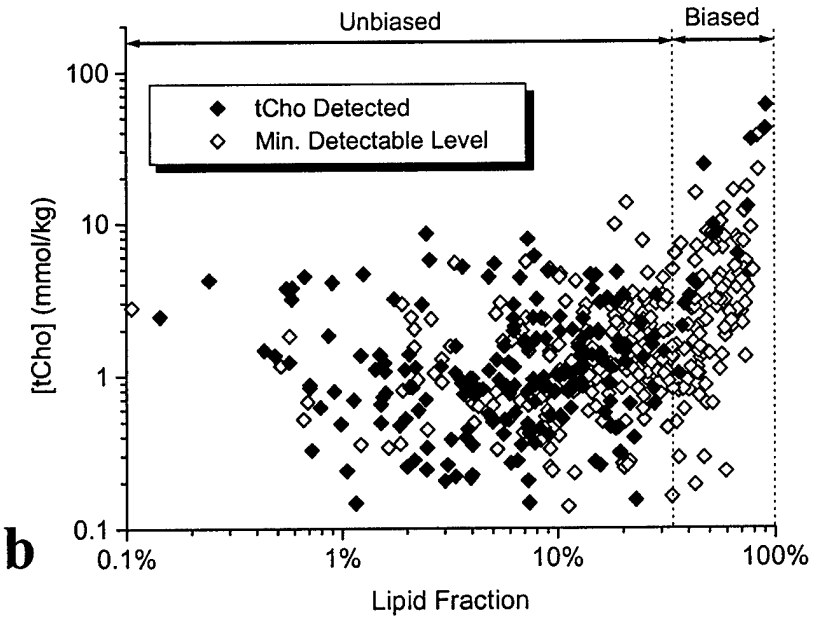
Unbiased
Biased
tCho Detected
Min. Detectable Level
[tCho] (mmol/kg)
100
10
1
0.1
0.1%
1%
10%
100%
Lipid Fraction

b

Figure 4

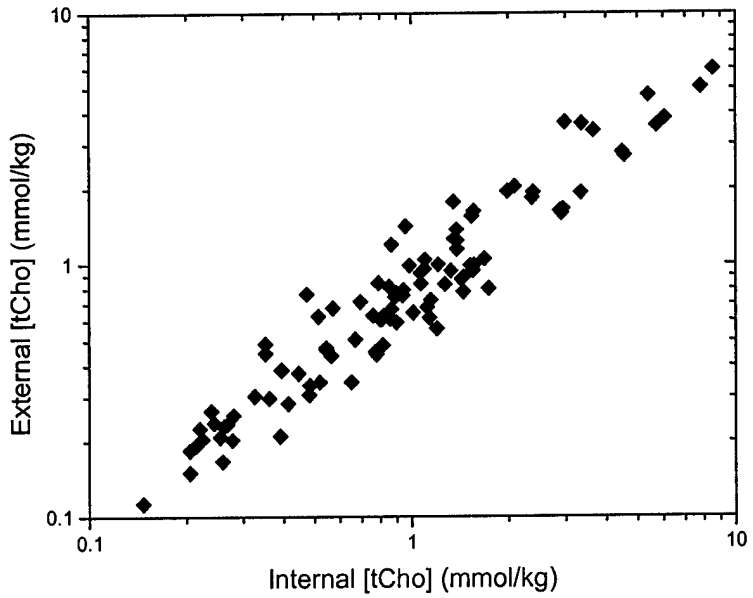

Figure 5

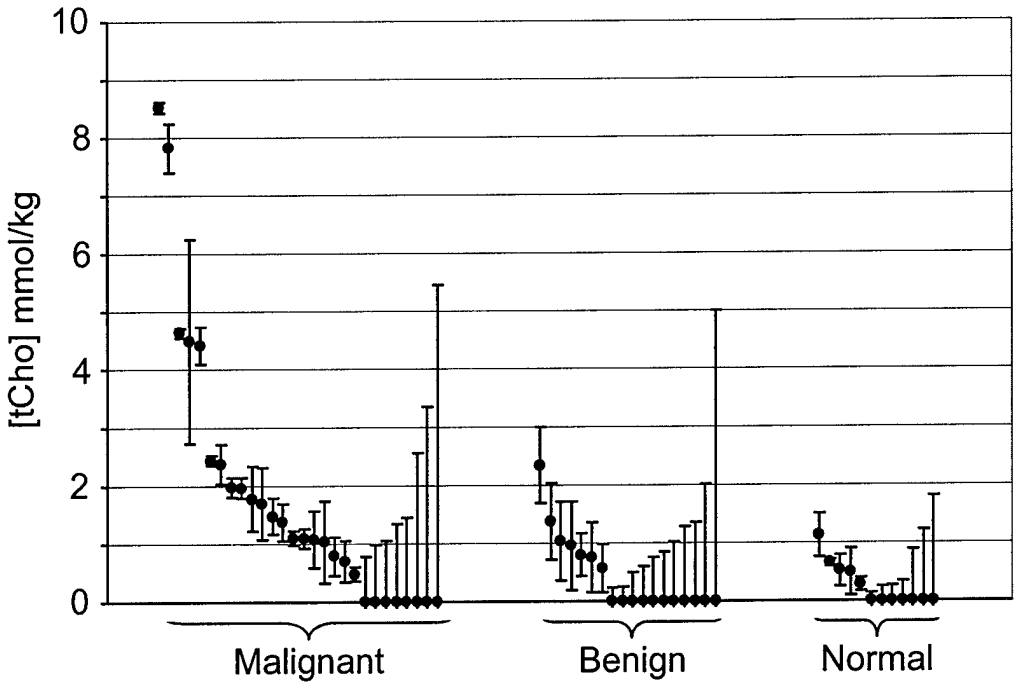

Figure 6

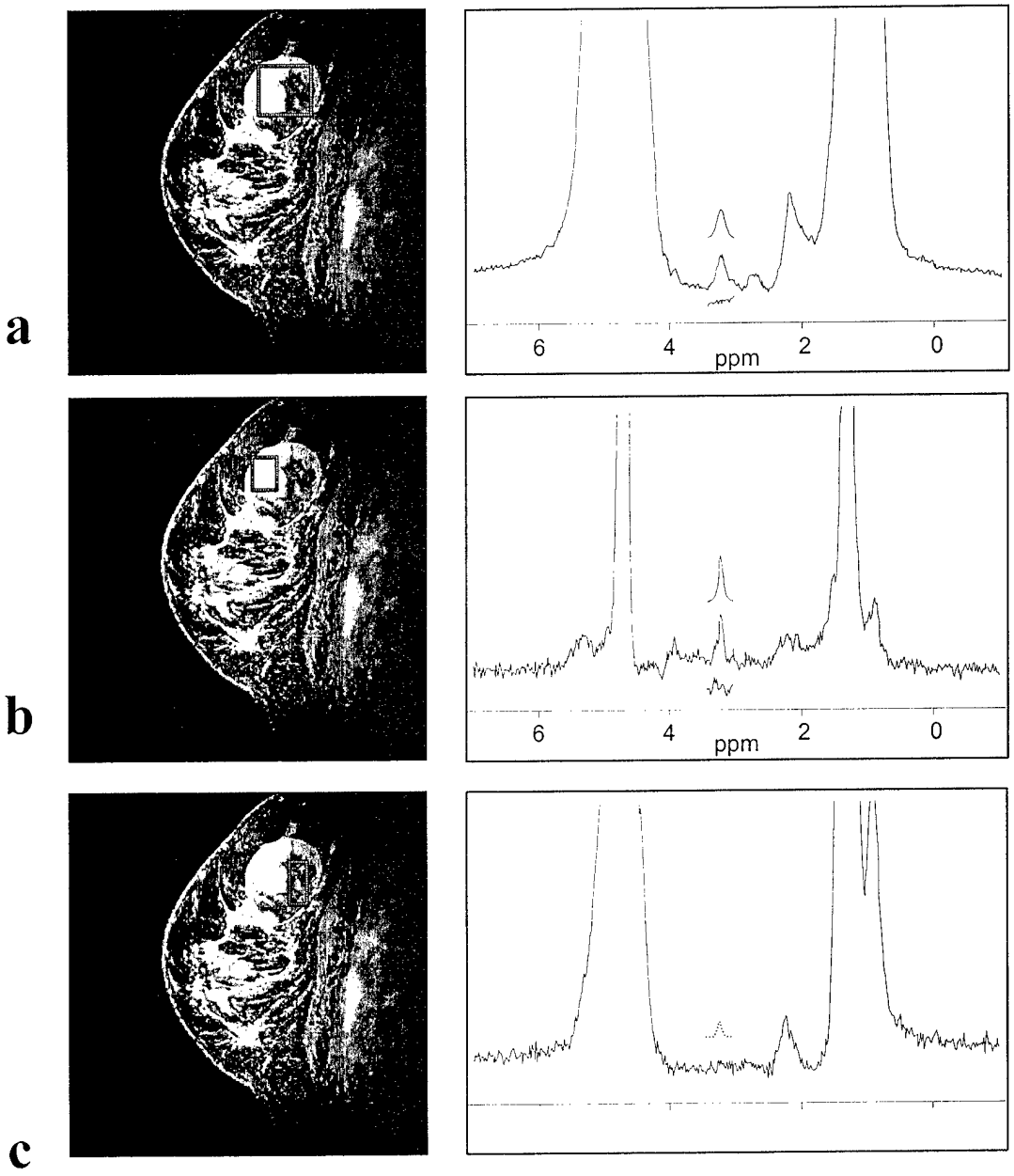

Figure 7